Chapter 7
Strategies for Plug-in Electric Vehicle-to-Grid (V2G) and Photovoltaics (PV) for Peak Demand Reduction in Urban Regions in a Smart Grid Environment

Ricardo Rüther, Luiz Carlos Pereira Junior, Alice Helena Bittencourt, Lukas Drude and Isis Portolan dos Santos

Abstract The strategy of using Plug-in Electric Vehicles (PEVs) for vehicle-to-grid (V2G) energy transfer in a smart grid environment can offer grid support to distribution utilities, and opens a new revenue opportunity for PEV owners. V2G has the potential of reducing grid operation costs in demand-constrained urban feeders where peak-electricity prices are high. Photovoltaic (PV) solar energy conversion can also assist urban distribution grids in shaving energy demand peaks when and where there is a good match between the solar irradiation resource availability and electricity demands. This is particularly relevant in urban areas, where air-conditioning is the predominant load, and on-site generation a welcome resource. Building-integrated photovoltaics (BIPV) plus short-term storage can offer additional grid support in the early evening, when solar irradiation is no longer available, but loads peak. When PEVs become a widespread technology, they will represent new electrical energy demands for generation, transmission and

R. Rüther (✉) · L.C.P. Junior · A.H. Bittencourt
Grupo de Pesquisa Estratégica em Energia Solar, Universidade Federal de Santa Catarina, Caixa Postal 476, Florianópolis, SC 88040-900, Brazil
e-mail: ricardo.ruther@ufsc.br

L.C.P. Junior
e-mail: pereira1435@gmail.com

A.H. Bittencourt
e-mail: alicehb_eel@yahoo.com.br

L. Drude
Universität Paderborn, Warburger Straße 100, 33098 Paderborn, Germany
e-mail: drude@nt.upb.de

I.P. dos Santos
Colégio Politécnico, Universidade Federal de Santa Maria, Campus UFSM, Santa Maria, RS 97105-900, Brazil
e-mail: isisporto@gmail.com

S. Rajakaruna et al. (eds.), *Plug In Electric Vehicles in Smart Grids*,
Power Systems, DOI 10.1007/978-981-287-299-9_7

distribution (GT&D) utilities. PEVs that are parked in the early evening can play the role of short-term energy storage devices for PV electricity generated earlier in the day. In a smart-grid environment, the combination of PEVs and PV can offer a good solution to assist the public grid. In this chapter, results on analyses of these strategies applied to selected urban feeders in the metropolitan area of a capital city in Brazil are presented. It is shown that, in a smart-grid environment, it should be possible to accommodate PEVs, BIPVs, V2G and the recharging of PEVs (grid-to-vehicle—G2V), and at the same time assist the urban grids and supply the new energy demands represented by the introduction of a PEV fleet, without compromising the existing grid infrastructure.

Keywords Photovoltaics · Plug-in electric vehicles · Vehicle-to-Grid (V2G) · Building-integrated photovoltaics (BIPV) · Smart buildings · Smart grids

7.1 Introduction

Among all human activities, transportation and energy generation are the two single largest contributors to greenhouse gas (GHG) emissions worldwide, and despite technological innovation leading to lower emissions per km or per kWh, total global emissions due to these activities keeps increasing every year. In this chapter the combined use of electric vehicles and on-site, building-integrated solar electricity generation in the context of smart grids are presented, in order to provide utility grid support both in terms of energy (kWh) and capacity (kW).

Plug-in Electric vehicles (PEVs) have been experiencing considerable development in recent years, and pure plug-in battery vehicles are now commercially available from a number of car manufacturers worldwide. PEVs have been proposed as a new power source for electric utilities in the US and Japan in the late nineties [1, 2]. Vehicle-to-grid power (V2G) uses electric-drive vehicles to provide power for specific electricity markets, since the electric power grid and light vehicle fleets are exceptionally complementary as systems for managing energy and power [3, 4]. A control signal from the grid operator can send a request for power to a large number of parked and plugged-in PEVs to feed energy to the grid. As information technology and battery technology evolve, the opportunities for PEVs to assist the public electricity grid in the V2G concept in a smart-grid environment become ever more real.

Electric drive vehicles (EVs) for V2G can be either hybrid, fuel cell, or pure battery vehicles (PEVs). They are all EVs in the sense that they all use an electric motor to provide all or part of the mechanical drive power. For V2G, each individual vehicle must have three required elements: (i) a connection to the grid for electrical energy flow, (ii) control or logical connection to allow for communication with the grid operator, and (iii) controls for metering on-board the vehicle. PEVs already have a grid connection to allow for charging, and the incremental costs and operational adjustments to add V2G are negligible [3, 4]. Furthermore, PEVs

have larger batteries (e.g. 24 kWh battery capacity for the Nissan Leaf[1]) than plug-in hybrids (e.g. 6–14 kWh for the DaimlerChrysler Sprinter[2]), or hybrid EVs (e.g. 1.6 kWh for the Toyota Camry[3]).

Among all renewable energy technologies, direct solar energy conversion or photovoltaics (PV) is the fastest growing segment in the energy generation industry [5]. In the last decade the PV industry annual production moved from megawatts to gigawatts, reaching the multi-gigawatt scale in the second half of the decade. The photovoltaic industry's compound annual growth rate (CAGR) from 2001 through the end of 2013 was 46 % [6]. In 2013 grid parity—when the cost of solar electricity becomes competitive with conventional, retail (including taxes and charges) grid-supplied electricity—was achieved in many places worldwide. Grid-connected PV used to be perceived as an energy technology for developed countries, whereas isolated, stand-alone PV was considered as more suited for applications in developing nations, where so many individuals still lack access to electricity. This rationale is based on the higher costs of PV, when compared with conventional, centralized electricity generation [7]. With the falling costs of PV and the increasing costs of conventional electricity, on-site PV generation became competitive with retail, end-consumer electricity prices also in many developing countries of the sunbelt.

The direct conversion of sunlight into electricity with grid-connected PV generators leads to a number of benefits to both the environment and the electricity system. The main technical advantage is the possibility of producing clean and renewable electrical power close to consumers or even at point of use, integrating PV generators on buildings or around urban areas. The peak shaving capability of distributed PV power systems reduces the strain on grid infrastructure [8–10]. A large number of distributed units for the same installed capacity allows for deferral of a bigger network investment. This favors small- to medium-sized urban PV systems [11]. The traditional utility concept relies on a relatively small number of fairly large and centralized power plants, which quite often are distant from the urban centers where energy is consumed. In large countries, transmission and distribution (T&D) infrastructure and associated losses are considerable, adding value to distributed PV power that goes beyond the value of the kilowatt-hour.

PV can contribute to a distribution utility's capacity if the demand peak occurs in the daytime period. Besides the advantage of peak demand reduction, PV systems will also contribute to a longer life of utility feeders [12]. Commercial regions with high midday air-conditioning loads have normally a demand curve in a good synchronism with the solar irradiance [9, 10, 13]. Another important factor in this analysis, is the comparison between the peak load values in summer and winter. The greater the demand in summertime in comparison with the demand in wintertime, the more closely the load is likely to match the actual solar resource.

[1] http://www.nissanusa.com/electric-cars/leaf/charging-range/battery/.

[2] http://www.epri.com/search/Pages/results.aspx?k=Plug-In%20Hybrid%20Electric%20Sprinter%20Van%20Test%20Program.

[3] http://www.toyota.com/toyota-owners-online-theme/pdf/Batteries2011-LowRes.pdf.

This is the typical picture of most capital cities in many sunny, developed and developing countries of the sunbelt, and the match between solar generation availability and power demands in urban areas is growing with the growing use of air-conditioning. Utility feeders in urban areas show distinct regions where commercial and office buildings dominate, and which present daytime peak demand curves, and residential regions where the peak demand values take place in the evening. To add value to the distributed nature of solar generated electricity, it is important to know the PV capacity of the different regions of a city when installing a PV power plant, in order to select the utility feeder with the greatest capacity credit. In this context, the concept of the Effective Load Carrying Capacity (ELCC) of PV was defined, to quantify the capacity credit of a strategically sited PV installation [8, 9, 13].

The widespread use of PEVs in urban environments will lead to considerably large new electrical energy demands, which will have to be met by new, and ideally distributed, power generation plants. Especially in large and sunny countries, solar PV conversion can meet these new electricity requirements, offering at the same time clean and renewable energy to alleviate the environmental impact of the transportation sector, and making the most of the distributed nature of the solar radiation resource in a distributed generation (DG) and smart-grid scenario. In this environment, the combination of PEVs and PV can offer a good solution to assist the public grid: (i) PEVs can offer grid support to urban feeders in the early evening through smart vehicle-to-grid (V2G) discharging strategies; (ii) BIPV can generate all the electricity needed to supply the new energy demands represented by PEVs and also offer grid support to urban feeders at daytime; and (iii) utilities can offer idle GT&D resources to recharge PEVs through smart grid-to-vehicle (G2V) recharging strategies in the early hours (00:00–06:00).

7.2 Urban Grid Electricity Demand Profiles, Electric Vehicles and Photovoltaics in a Smart Grid Scenario

In most urban centers, due to the extensive use of air-conditioners and electric resistance showerheads for water heating, energy demand peaks in the late afternoon/early evening, from 19:00 to 21:00 [14, 15]. Distribution utilities impose prohibitively high tariffs to business and industry in this period to avoid even higher power demands. These demand peaks coincide with the typical urban driver weekday habits of returning home from a working day. Figure 7.1 shows the typical load curve of a specific urban feeder in the Brazilian metropolitan area of Florianópolis-SC [16]. In this example, the local distribution utility needs to provide a costly energy supply infrastructure to cover the 5-h period from 17:30 to 22:30. This additional capacity remains idle for most of the day and represents a considerable investment from the distribution utility, which is passed on to electricity consumers as a component of the electricity tariff. While the potential contribution of PV in the peak hours shown in this example is limited, charging PEVs with solar electricity while

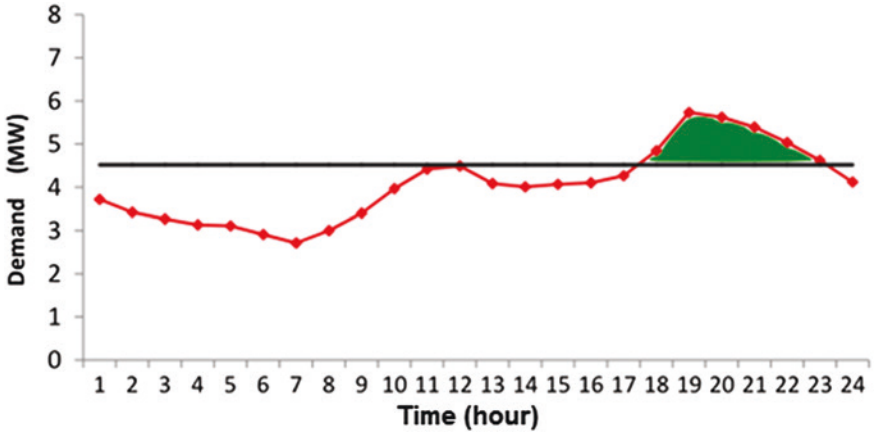

Fig. 7.1 Typical load curve of urban utility distribution feeder TDE05 in Florianopólis-SC, Brazil. With vehicle-to-grid (V2G) strategies in a smart-grid environment, a fleet of PEVs can assist the grid in reducing the evening peak (*green area*), while solar electricity generation with PV integrated on buildings can provide the additional electricity requirements resulting from the introduction of PEVs

they are parked at home or at work, and using a fraction of that electricity to feed the utility's grid and alleviate the load at peak hours has become a technically viable alternative with the advent of the smart-grid. In a smart-grid scenario, with PEVs and grid-connected PV integrated on buildings, the potential contribution of PEVs to assist in shaving the load peaks of a distribution utility feeder at peak hours can be assessed. Furthermore, the potential of PV to supply or complement the additional energy requirements represented by the incorporation of a number of PEVs to the urban fleet in a specific utility feeder area in the metropolitan region of small and large cities can also be proposed and evaluated.

The distribution utility feeder TDE05, for which Fig. 7.1 shows a load curve on a typical day, supplies energy to a mixed residential/commercial/university area. Figure 7.2 shows a color contour map with the hourly demand profile of this feeder for all the 8,784 h of the year, where a distinct peak (warmer colors) is noticeable in the early evening all over the year, from before 18:00 to after 22:00. The figure also shows that during the early hours from 00:00 to 06:00 the feeder is underutilized and therefore technically able to supply energy to recharge a considerable amount of PEVs. Furthermore, Fig. 7.2 shows that during daytime hours the feeder is able to receive large amounts of PV-generated electricity from grid-connected, building-integrated PV generators installed in the area covered by this particular feeder. In the early evening, however, when solar PV generation is no longer available, a fraction of the surplus electricity stored in the batteries of parked and plugged PEVs can be made available for grid support. Figure 7.3 shows a schematic diagram of this concept. The daily urban commute in the metropolitan area of Florianópolis is very typical and representative of many metropolitan areas around the globe, where the driver leaves home for work in the early

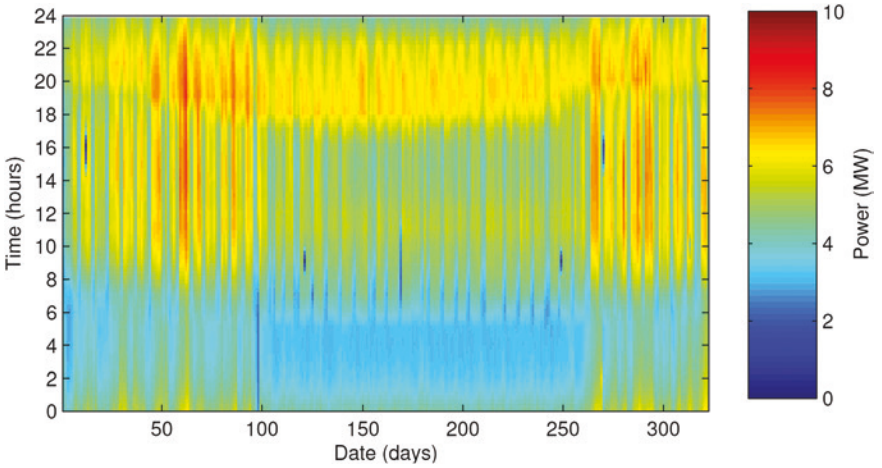

Fig. 7.2 Original energy demand profile of the urban feeder TDE05 (in MW) in Florianópolis for the 8,784 h of the year

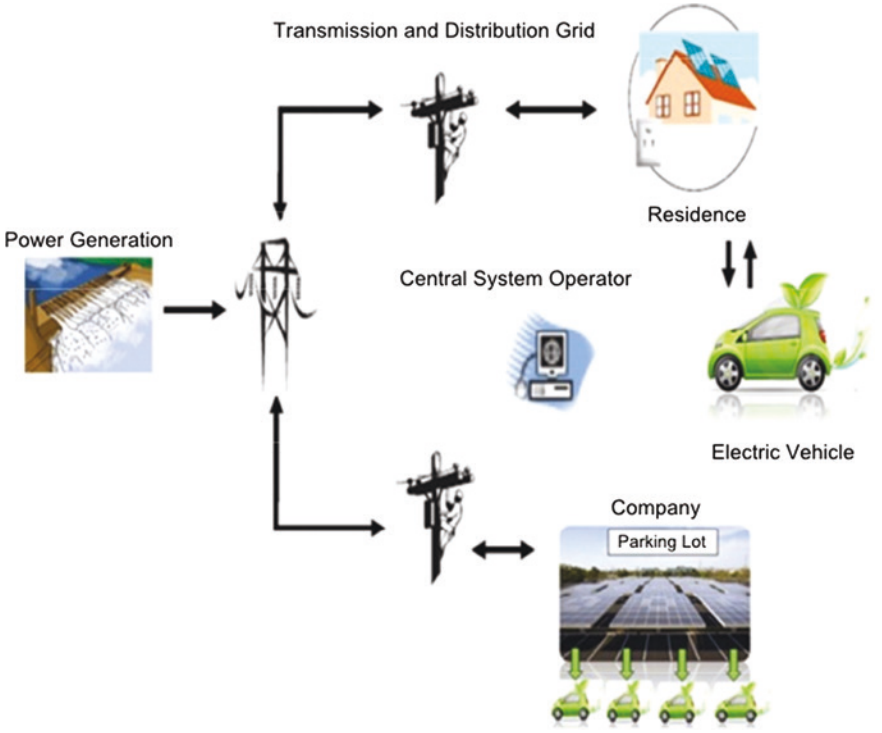

Fig. 7.3 Schematic diagram of the interaction of solar PV generators and PEVs with the public electricity grid in a smart-grid environment

morning, driving for some 20 km on average, and leaving the car parked all day long. In a smart-grid, BIPV and PEV environment, this vehicle could be parked under a PV-covered car parking lot. Distribution utility feeder characteristics and load profiles can vary depending on a number of aspects ranging from climatic and seasonal effects (heating and cooling loads), user characteristics (residential, commercial, business/public, industrial), among others, and the effects of using both building-integrated PV and the energy available in PEVs batteries to flatten the feeder's load curve are a matter of growing interest. Figure 7.4 shows a real, typical and original load curve of the previously shown distribution utility feeder on a particular day. The figure also shows the peak-shaving effect of a number of PEVs assisting this feeder at peak hours in the evening (blue triangles), the contribution of PV solar generation at day-time (green diamonds), and the recharging of the PEV fleet during the early hours (brown circles), when conventional, centralized generators operate at partial load conditions.

Figure 7.5 shows, as an example for the month of March 2008 and on a daily basis, the total maximum number of PEVs that can (top) participate in assisting the corresponding feeder with peak-shaving in the evening (V2G), and (bottom) be recharged in the early hours (G2V) without imposing the need of any upgrade in the existing urban distribution system. The number of vehicles involved in both V2G and G2V shown in these figures is considerably smaller than the existing vehicle fleet available in the corresponding area. In a smart-grid environment,

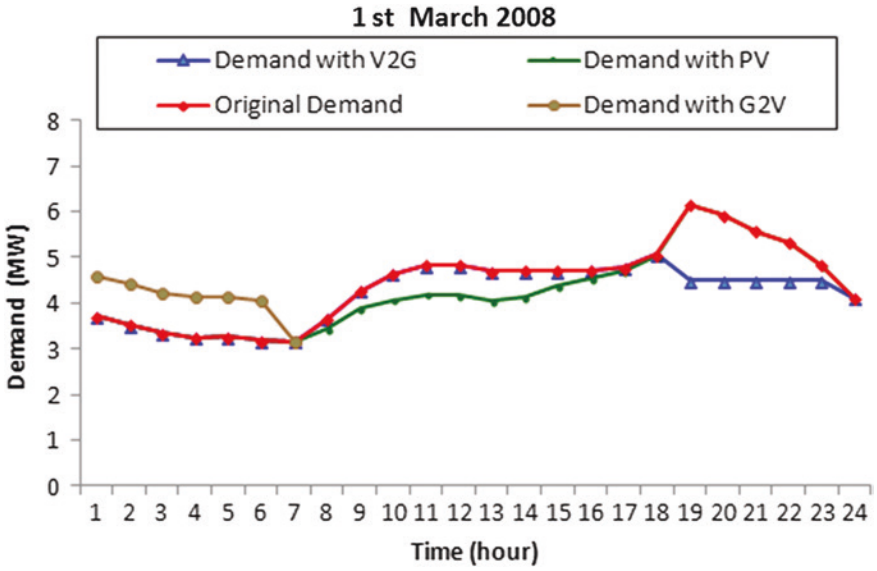

Fig. 7.4 Original demand profile for the distribution utility feeder TDE05 in Florianópolis—Brazil (*red circles*), and the potential contribution of PV (*green diamonds*) for daytime hours peak-shaving, PEVs for evening hours peak-shaving (*blue triangles*), and the corresponding load for PEV recharging in the early hours (*brown circles*)

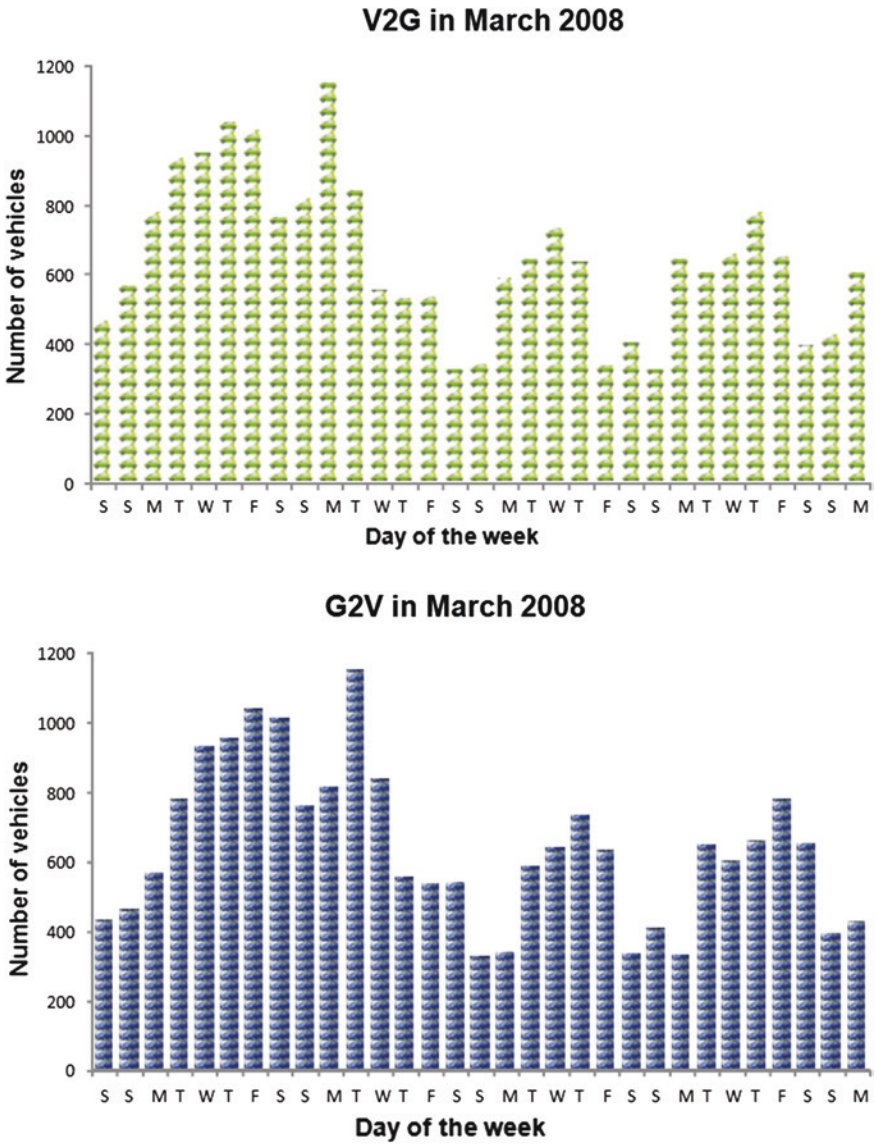

Fig. 7.5 Maximum number of PEVs that the distribution utility feeder TDE05 can take on a given day in March 2008, for evening peak-shaving V2G discharging (*top*), and early hours G2V recharging (*bottom*)

parked and plugged PEVs will participate in V2G and G2V energy transfer transactions in a first-come, first-served priority order.

Central System Operators all over the world struggle to maintain a load curve as flat and constant over the day as possible. With the advent of the smart grid, PEVs that allow for V2G, and distributed rooftop PV in residential, commercial,

industrial and public buildings are faced with both an opportunity, but also new challenges, in dispatch and control. While the conventional utility concept relies on a relatively small number (typically up to a few thousands), of fairly large and centralized generators and power plants (in the hundreds of megawatts up to the gigawatts level) that can be dispatched when needed, the decentralized generation paradigm consists of millions of dispersed and small power plants, most of which are intermittent in nature and cannot be dispatched in a controlled way. As the penetration level of these new and dispersed generation units increases, Central System Operators also need to introduce new control strategies for effectively profiting from decentralized generation.

7.3 Photovoltaics in Buildings for PEV Recharging and Grid Support

PV solar energy conversion to electricity has been the fastest growing segment of the electricity generation market in the last seven years, and in 2013, for the first time, the world added more solar PV than wind generating capacity [5]. The consistent cost reduction experimented by the PV industry as a consequence of volume markets, associated with the possibility of installing PV generators directly at the point of energy use, and the development of PV modules suited for building integration, make PV an ideal technology for deployment in the urban environment [17, 18]. Large-scale, centralized PV generation is an area-intensive technology, but dispersed, building-integrated and building-applied photovoltaics (BIPV and BAPV) constitute a most elegant way of generating considerable fractions of urban electricity, without the need of dedicating exclusive surface areas for PV plant installations. While in BIPV generators either conventional or tailor-made PV modules become an integral part of the building envelope, replacing roofing tiles or other building elements; BAPV systems are more typically used in retrofits, with off-the-shelf PV modules mounted on a separate metal support structure, superimposed on an existing building's roof. In any case, the building envelope (roofs and façades) provides the surface area for the PV plant at premium urban locations in many cases; the building's electrical installation provides the electrical interface of the PV plant to the public utility grid. Energy is generated at very close proximity to the end user, avoiding the infrastructure investments and losses related to transmitting and distributing electrical power, since in most of the cases no extra infrastructure requirements need to be provided for connecting a BIPV or a BAPV plant to the grid. There are additional benefits of scattering PV generators in the urban environment, since PV can also offer distribution utilities ancillary services such as grid support and demand peak shaving, especially when there is a good match between the solar energy resource availability and electricity loads (e.g. air-conditioning loads) [8, 10, 13, 18–23].

In order to optimize the annual output performance of PV generators on buildings, PV array orientation (azimuth) and tilt angle are a major concern, as system

design and electrical configuration must maximize sunlight exposure. A number of studies have been carried out on the performance of PV generators at various orientations and tilt angles for different latitudes [24, 25]. Ideally a PV generator should be oriented towards the equator, and at a tilt angle close to the site latitude. Low-latitude sites will be less sensitive to azimuth deviations for low tilt angles on roof-mounted PV generators, and high-latitude sites will have lower energy output losses for PV generators on vertical façades [25]. Single-family detached homes in residential suburbs can be considered the most suitable building stock for BIPV and BAPV generators, due to their typically large roof areas and small mutual shading effects, while residential and commercial multistorey buildings will often represent challenging aspects in PV system output optimization [26–30], as well as in assessing the incoming solar irradiation resource availability [31].

7.3.1 The Potential of Residential and Public Building Rooftop PV in Supplying the Additional Energy Requirements of a PEV Fleet in a Smart Grid Environment

The widespread uptake of PEVs in urban areas brings new challenges to both the electricity distribution supply and control, and the new energy requirements represented by a fleet of PEVs needs to be assessed. In this section, the potential of a stock of residential buildings with rooftop PV integration in supplying the energy needs of a defined number of PEVs is presented. The existing buildings rooftops of both the residences where the PEVs will be plugged-in during the evening and early hours, as well as large-area public buildings (the local distribution utility headquarters building and the local university theater building), which are served by the same feeder, are presented and assessed. The study was carried out for both thin-film amorphous silicon (a-Si) and traditional crystalline silicon (c-Si) PV modules [32]. On the University campus alone, the potential for integrating PV on existing, large-area rooftops is larger than 3 MWp for a-Si, and larger than 6.7 MWp for c-Si. Using a typical annual energy yield of 1,200–1,300 MWh/MWp for Florianópolis, the annual PV electricity production potential of these areas is over 3,600 MWh for a-Si and 8,040 MWh for c-Si. This is enough to supply electricity to a PEV fleet of some 1,800 cars using a-Si, and over 4,000 cars using c-Si PV modules. The next step in the assessment is to investigate (i) the effects of making hundreds (400–600) of PEVs available to assist this particular utility feeder in the urban distribution grid from 19:00 to 24:00; (ii) the effects of introducing a certain amount (e.g. 1 MWp) of grid-connected, building-integrated PV to generate enough energy to cover the new energy demands represented by the new EV fleet, and at the same time assist the utility feeder during daytime hours; and (iii) the capacity of, and the effects on, the utility feeder in recharging the PEV fleet during the early hours (00:00–06:00). A typical 4 kW PEV battery charger to recharge the Nissan Leaf 24 kWh EV battery in up to 6 h is assumed.

The first grid-connected, building-integrated PV system in Brazil was installed at the Solar Energy Laboratory at Universidade Federal de Santa Catarina in Florianópolis in 1997 [33, 34]; this PV generator includes a comprehensive data acquisition system that has been continuously logging electrical performance, ambient and PV module temperature and plane-of-array and horizontal solar irradiation data at 5-min intervals [19, 33, 34]. The annual global horizontal solar irradiation resource averages some 1,550 kWh/m^2/year, and there are a number of PV installations at various orientations and tilt angles being continuously monitored and assessed, with detailed output performance, ambient and PV module operating temperature, and irradiation data available. Two of these PV systems were used as a reference to establish the baseline for the typical output performance of traditional c-Si and thin-film a-Si PV generators with ideal orientation and tilt angle. Both PV systems are oriented towards the Equator (true North), at latitude tilt (27°), with no shading effects from dawn to sunset. The 2.25 kWp c-Si PV system operates on the roof top of the local Utility Eletrosul Energy Efficient House (Fig. 7.6), and the a-Si PV system is installed on the Universidade Federal de Santa Catarina's Theater building (Fig. 7.7). Real operational performance data (electrical output generation values at 5-min intervals) collected from these two reference PV installations have been used to calibrate the PV output simulation method used to assess the potential generation capacity, in kWh generated per kWp installed, of all PV generators presented in this chapter. Figure 7.8 shows the monthly energy generation (in kWh/kWp), of the two reference PV systems, and also the measured monthly global radiation (in kWh/m^2).

Fig. 7.6 Traditional crystalline silicon (c-Si) rooftop PV system at the Energy Efficient House, in Florianópolis, Brazil (27°S latitude). The PV generator faces true North, and is tilted at 27°

Fig. 7.7 Thin-film amorphous silicon (a-Si) rooftop PV system at the UFSC's University Theater, in Florianópolis, Brazil (27°S latitude). The PV generator faces true North, and is tilted at 27°

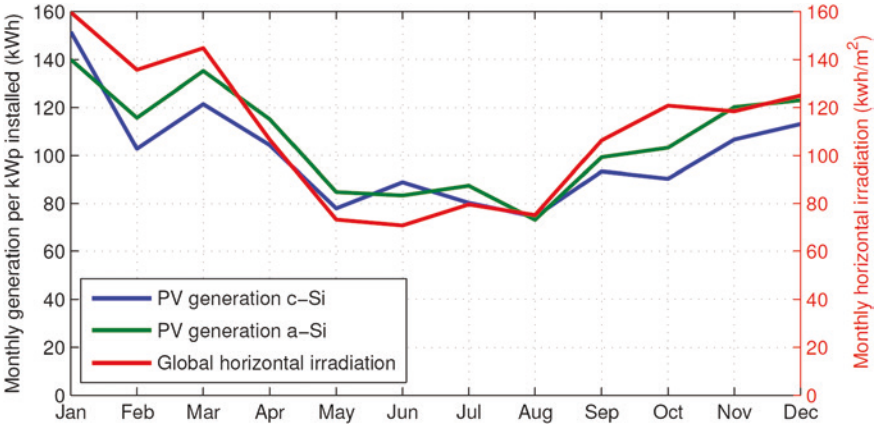

Fig. 7.8 Monthly average of the global horizontal irradiation (*green dotted line*, in kWh/m^2), PV energy generation (in kWh/kWp) of the traditional c-Si PV system (*blue solid line*), and thin-film a-Si PV system (*red dashed line*) operating in Florianópolis, Brazil (27°S latitude)

A typical urban area was selected to study the PV roof integration potential of PV kits on single-family residential houses, and the resulting energy generation potential of the proposed PV generators was established. The urban area under study is a mixed residential-commercial area, with a predominance of detached, single-family, one- or two-storey houses, with negligible mutual shading effects

on roof covers. As previously shown in Fig. 7.1, the electricity demand of the utility feeder supplying energy to this area presents two peaks, with an early evening peak around 19:00, and a second peak close to midday.

The next step consisted in analyzing the available rooftop surface area, orientation, and tilt angles of this complete building stock, in order to determine the availability of suitable areas for PV integration. The GEO map (Corporative Geoprocessing Map), supplied by the city council was used to obtain the residential sample size determination of that urban zone, which is comprised of 496 single-family houses. This information was also compared with the orthoimage of the area for the same year, in order to ascertain that the energy demand, solar irradiation availability, and land occupation characteristics all corresponded to the same period. It was assumed that the PV kits defined in this study have an area small enough to fit on the residential buildings studied, and a conservative 7.5 % error margin was adopted. The sample size determination (n) of the selected residential buildings is a function of the total number of total residential houses (N), confidence level (Z = 95 %), probability to find available area for PV kits on residential rooftops (p = 95 %, with q = 1–p), and error margin (E = 7.5 %), it was obtained from Eq. 7.1 as follows:

$$n = \frac{N \cdot Z_{\alpha/2}^2 \cdot p \cdot q}{E^2 \cdot (N-1) + Z_{\alpha/2}^2 \cdot p \cdot q} \tag{7.1}$$

$$n = \frac{496 \cdot 1,96^2 \cdot 95 \cdot 5}{7,5^2 \cdot (496-1) + 1,96^2 \cdot 95 \cdot 5}$$

With the resulting n = 30.5, the roof cover blueprints of 31 residential houses were requested and obtained from the city council's Urban and Public Services Municipal Bureau, for a more detailed roof cover area availability analysis.

Two pre-defined PV kits were designed and proposed for the integration of a-Si or c-Si PV technologies on all of the residential buildings rooftops. These BAPV generators were sized in order to be small enough to fit on the roofs considered in this study, and large enough in order to be able to supply a considerable fraction of the electricity demands in each house. It was also defined that both PV kits should have a similar total surface area, so that the aesthetic appearance of both types of installation would also be similar. The solar-to-electricity conversion efficiency of the thin-film a-Si PV technology is about half the efficiency of the more traditional c-Si PV technology. As a consequence, for a similar surface area, an a-Si PV kit will have about half the nominal power of a c-Si PV kit. Since the current price of turn key PV generators for small, residential PV installations, can be considered independent of the PV technology selected, this decision resulted in the a-Si PV kit costing about half the price of the c-Si PV kit. The a-Si PV kit considered in this study is rated at 0.5 kWp nominal DC power, uses four 5.0 × 0.4 m^2, 125 Wp PV modules, with a total surface area of 8.0 m^2. The c-Si PV kit is rated at 1 kWp nominal DC power, uses five 1.42 × 1.00 m^2, 200 Wp PV modules, and has a total

surface area of 7.1 m^2. An 8.0 m^2 area was thus defined as a minimum roof area availability requirement for PV kit integration.

Each of the 31 sample building roof cover areas was individually analyzed for the PV integration potential, taking into account the land block area and orientation, as well as the existing roof orientation and tilt, and the availability of the minimum 8.0 m^2 area required for PV kit integration, oriented as much as possible towards the Equator (true North). This analysis resulted in a number of different possibilities for PV kit roof integration on these existing roof covers, with all the 31 houses presenting an 8.0 m^2 roof cover area suitable for PV kit integration. It was then assumed that all of the 496 houses were able to accommodate either of the PV kits, and the PV generation potential was then calculated in each case, to be further compared with the energy demand profile of the corresponding area in the suburb.

The expected PV energy generation for different orientations and tilt angles was determined based on three factors: (i) the residential houses' roof area availability, orientation and tilt angles, (ii) the individual houses' solar irradiation resource availability, which was calculated in each case from the available global horizontal irradiation data for the plane-of-array of each roof orientation and tilt angle; and (iii) the output performance of the reference a-Si and c-Si PV generators operating in the same area. Electricity consumption was estimated from the values obtained from the local utility and adjusted to the 496 houses analyzed.

Equation 7.2 was then used to estimate the energy generation potential E (in kWh) of the PV kits with an installed capacity P (in kWp), when installed on all the existing roof covers (n = number of samples), based on the corresponding reference output performance for each PV technology (GerSist, in kWh/kWp), and taking into account a reduction factor due to their non-ideal orientation and tilt angles (Def = 0.942). A weighted average of all roof orientations and tilt angles was used to calculate this Def output reduction factor, which was statistically determined as further explained.

$$E = n \cdot P \cdot GerSist \cdot Def \tag{7.2}$$

In order to obtain the generation value (GerSist), the measured output power of the two reference PV generators used to calibrate the simulation of the PV generation potential were compared. Figure 7.8 shows that the thin film a-Si PV system (annual energy yield = 1,280 kWh/kWp/year) generates more energy (>6 %) on an annual basis than the c-Si PV installation (annual energy yield = 1,205 kWh/kWp/year). Figure 7.8 also shows the profile of the monthly PV generation (in kWh/kWp) of the two PV systems, together with the solar irradiation levels for the same period (in kWh/m^2). It can be clearly seen that the thin-film a-Si PV generator is a better performer overall, especially during summer months. The reasons for this behavior are related to the lower temperature coefficient on power of a-Si when compared with c-Si; to a spectral content of sunlight in summer months more suited to the spectral response of a-Si devices; and to the partial annealing of the Staebler-Wronski effect [35], and have been described in detail elsewhere [36, 37]. Also noteworthy is the fact that the energy output in

summer months is almost double of that during the winter, in accordance with the solar irradiation availability at the site.

As shown by the blue diamonds in Fig. 7.9, the 31 houses sample analyzed in this chapter present more variations in roof cover orientation than in tilt angle. Roof tilt angle is associated with roofing tile model, and in this suburb most houses use the typical red clay tiles, tilted between 15° and 35°. Roof orientation, on the other hand, varies according to the urban grid design and architectural concepts, and is therefore more prone to larger variations. In this analysis, the 31 sample roof orientations and tilts studied in detail, were extrapolated to the 496 existing houses. The various roof orientations and tilt angles of the house sample studied will lead to varying and specific output performance behaviours of PV generators installed on each of these roofs, which are represented by the "Def" parameter in Eq. 7.2. Figure 7.9 also allows for a rapid and efficient visualization of the expected PV generator performance on any particular roof orientation and tilt, with respect to the maximum theoretical performance of an ideally oriented and tilted PV generator. The graph is based on irradiation values calculated using the RADIASOL software [38]. This software calculates the incoming solar irradiation levels at any surface orientation and tilt angle, based on the local daily averages of the monthly global horizontal irradiation. In this chapter, solar irradiation vales obtained from the SWERA project [39] were used to calibrate the RADIASOL software. In Fig. 7.9, maximum (100 %) output corresponds to the performance of a rooftop PV generator with ideal roof orientation (facing true North in the Southern Hemisphere) and tilt angle (latitude tilt = 27° for the city of Florianopolis), with the corresponding output for all the other possible orientations

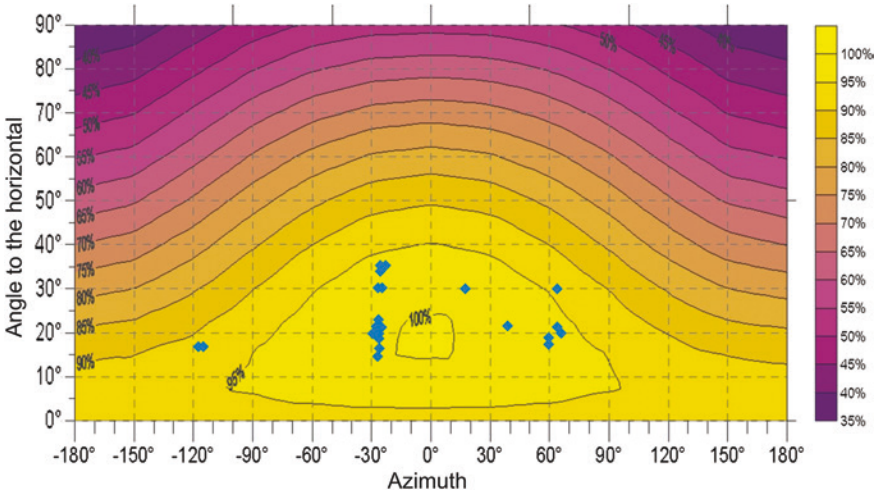

Fig. 7.9 Distribution of surface area availability for PV kit integration according to orientation (azimuth deviation) and tilt angle of the 31 residential house roof covers (*blue diamonds*), with percentage of the maximum annual PV generation potential as a function of their position in Florianópolis, Brazil (27°S latitude)

(azimuth deviations from −180° to +180° off true North), and tilts (varying from horizontal roofs = 0°, to vertical walls = 90°) being easily visualized.

Since the variance is unknown and the sample (n) is small, variances (F) in orientation and tilt angle were analyzed statistically using Eq. 7.3, to determine deviation averages, with Sx and Sy representing the sample's deviations for the small sample (n). Because most of the azimuthal deviations are statistically similar, Eq. 7.4 was used to estimate the weighted deviation (Sp) from average; Eq. 7.5 was used to determine the deviation from the difference among averages (Sw); Eq. 7.6 was used to calculate the Student's (t) distribution value; and Eq. 7.7 was used to compare t with the samples' distribution, and determine whether the averages could be considered equal at a 95 % confidence level.

$$F = \frac{Sx^2}{Sy^2} \tag{7.3}$$

$$Sp = \sqrt{\frac{(n_x - 1) \cdot Sx^2 + (n_y - 1) \cdot Sy^2}{n_x + n_y - 2}} \tag{7.4}$$

$$Sw = Sp\sqrt{\frac{1}{n_x} + \frac{1}{n_y}} \tag{7.5}$$

$$|t| = \frac{\bar{x} - \bar{y}}{Sw} \tag{7.6}$$

$$|t| = t_{\frac{\alpha}{2}}(n_x + n_y - 2) \tag{7.7}$$

The statistical analysis of the average incident solar irradiation level distribution at different azimuth angles, demonstrated that both at the ideal latitude tilt angle of 27°, and also at a more steep 45° tilt angle, deviations are similar, and there is no significant difference in average solar irradiation levels among azimuth deviations of 5°, 10°, 15°, 20°, 30°, 45° and 90°, for a 95 % confidence level.

The statistical analysis has also demonstrated that regarding tilt angles, for North-oriented (South-oriented in the Southern hemisphere) planes tilted up to 20°, there is no significant difference in averages or standard deviations at this low latitude. From tilt angles larger than 30°, averages are still similar up to 45°, but standard deviations can no longer be considered similar. For 90° tilt angles (vertical façades), both averages and standard deviations are different and cannot be compared. Since the statistical analysis did not reveal considerable differences in solar irradiation levels among the existing roof covers evaluated, a 10° step in tilt angle and a 30° step in azimuth angle variations were adopted in Fig. 7.9. The 100 % generation level in the graph corresponds to an average yearly output of 1,280 kWh/kWp for the a-Si PV technology, and 1,205 kWh/kWp for the c-Si PV technology installed in Florianopolis (GerSist, value in Eq. 7.2 corresponding to

640 and 1,205 kWh/year for the 0.5 kWp a-Si and 1.0 kWp c-Si kits respectively). For any other combination of orientation and tilt angles, *ceteris paribus*, average annual energy generation yields can be derived from Fig. 7.9. Monthly electricity demand data were obtained from the local distribution utility for the TDE05 feeder. The data obtained were peak demand measurements for each 15 min for all days of the year, from which daily demand curve averages, total consumption and also peak power demand were calculated.

After identifying the orientation and tilt angles of the 496 roof covers, and using the graph shown in Fig. 7.9 to assess their corresponding output performance, the PV kits generation potential was estimated as a fraction of the maximum potential verified for ideally oriented and tilted PV generators. Figure 7.9 also shows that 87 % of the PV kits will be able to generate at least 95 % of the maximum theoretical output for Florianópolis; about 10 % will be able to generate at least 90 % of the maximum possible; and only about 3 % of the PV kits will generate at least 85 % of their maximum potential. The averaged annual energy generation yield of the 496 PV kits proposed to be installed on these existing house roof covers, resulted in 94.2 % ("Def" parameter in Eq. 7.2) of the maximum theoretical potential. These results are significant, because they demonstrate that retrofitting PV kits to existing individual residential house roof covers which were not originally designed to integrate PV generators, leads to the majority of the BAPV installations to perform at a level which is very close to their maximum theoretical potential. From Fig. 7.9 it is clear that for low-pitched roofs (<10°) at this latitude, any roof orientation will lead to at least 90 % of the maximum theoretical energy generation potential. Figure 7.10 shows the potential electricity generation of the BAPV kits in three scenarios, namely:

- Scenario K1: All the 496 houses fitted with 1.0 kWp PV kits using the c-Si PV technology. Installed PV capacity = 496 kWp (In Eq. 7.2: n = 496; P = 1; GerSist = 1,205; Def = 0.942);
- Scenario K2: All the 496 housed fitted with 0.5 kWp PV kits using the thin-film a-Si PV technology. Installed PV capacity = 248 kWp (In Eq. 7.2: n = 496; P = 0.5; GerSist = 1,280; Def = 0.942);
- Scenario K3: Half (248) of the houses fitted with the 1.0 kWp c-Si PV kit, and the other half (248) of the houses fitted with the 0.5 kWp thin-film a-Si PV kit. Installed capacity = 372 kWp (In Eq. 7.2: n1 = 248; P1 = 1; GerSist1 = 1,205; n2 = 248; P2 = 0.5; GerSist2 = 1,280; Def = 0.942).

Following the analysis of PV kit installations in a BAPV configuration, the whole roof cover areas of the residential houses sample were evaluated in order to determine the PV generation potential in a BIPV configuration, with tailor-designed PV systems for each house. While the BAPV alternative results in economies of scale due to PV kits standardization and volume production, the BIPV option results in an optimized deployment of the existing roof cover areas, leading to net energy-positive buildings. The nearly 80,000 m^2 surface areas available on these existing roofs corresponds to a PV capacity of nearly 5 MWp for the thin-film a-Si PV technology, and over 11 MWp for the more traditional c-Si PV technology.

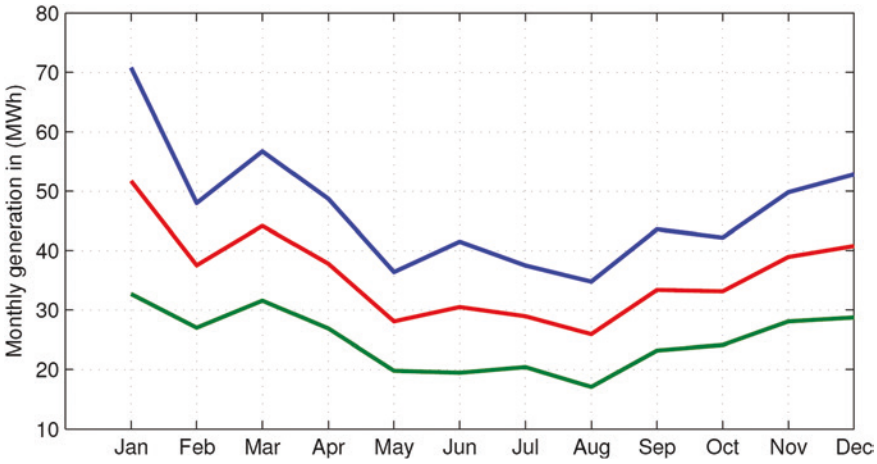

Fig. 7.10 Monthly PV energy generation potential (in kWh/month) under Scenarios K1 (496 units of the 1.0 kWp c-Si PV kit), K2 (496 units of the 0.5 kWp a-Si PV kit) and K3 (248 units of the 1.0 kWp c-Si PV kit and 248 units of the 0.5 kWp a-Si PV kit)

Assuming the average solar generation potential for the areas considered, this installed capacity translates into an annual energy generation potential of some 5,800 MWh/year for the thin-film a-Si PV technology, and around 12,300 MWh/year for the c-Si PV technology, when installed in a BIPV configuration on all of the available areas of the 496 existing houses in this suburb. This is enough to supply electricity to a PEV fleet of some 2,900 cars using a-Si, and over 6,100 cars using c-Si PV modules, which by far exceeds the total fleet of vehicles registered in this suburb.

7.3.2 The Potential of Rooftop PV and PEV Vehicle-to-Grid (V2G) Strategies in Peak Demand Reduction in Urban Areas in a Smart Grid Environment

In order to establish the potential of rooftop PV in a public building in both supplying the additional energy requirements of a PEV fleet, and in providing grid support to the local utility in a smart grid environment, the local public utility Eletrosul Headquarters building in Florianópolis was studied. Figure 7.11 shows the 1 MWp solar PV installation integrated on both the building's roof (450 kWp) as well as in the surrounding parking areas (565 kWp distributed in nine parking canopies). In order to evaluate the best energy flux strategies over a daily period, three phases were defined along the 24-h period, namely: Phase 1—daytime (solar PV feeding the Eletrosul Headquarters building + V2G from the parked PEV fleet to the Eletrosul Headquarters building); Phase 2—nighttime (V2G from the parked PEV fleet to the Eletrosul Headquarters building at peak demand hours);

Fig. 7.11 Aerial view of the Eletrosul Megawatt Solar PV plant in Florianópolis, Brazil (27° South), showing the (450 kWp) rooftop and the nine parking canopies (565 kWp), which comprise the 1 MWp solar power plant

and Phase 3—nighttime (G2V from PEV owners residence power sockets to recharge PEVs in the late night and early hours). Figure 7.12 shows a schematic diagram with these three phases distributed over the 24-h period. Phase 1 is the longest period, when sunshine is available, and when the PV generator assists the building owner (and the distribution utility) in reducing the power demand from the grid and in modulating the load curve; in case of PV generation reduction caused by unfavourable meteorological conditions, parked and plugged-in PEVs

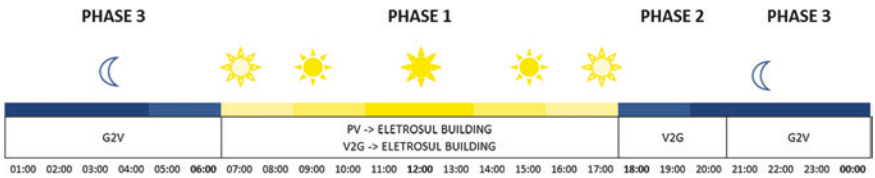

Fig. 7.12 Definition of the three phases in which different energy management strategies are applied, namely: *Phase 1*—daytime (solar PV feeding the Eletrosul Headquarters building + V2G from the parked PEV fleet to the Eletrosul Headquarters building); *Phase 2*—nighttime (V2G from the parked PEV fleet to the Eletrosul Headquarters building at peak demand hours); and *Phase 3*—nighttime (G2V from PEV owners residence power sockets to recharge PEVs)

can assist in this task with V2G, contributing to grid reliability. Phase 2 is the shortest period, and coincides with the distribution utility's load peak; this is the period in which V2G is most valuable, as end-user tariff rates can be 10 times as high as in off-peak periods. Phase 3 is also considerably long, when most of the generation, transmission and distribution assets are idling because of low power demand from the grid, and is therefore ideal for PEV recharging due to low tariff rates and abundant grid resource availability. The combination of daytime solar electricity generation and both daytime and nighttime V2G electricity injection can thus effectively assist in reducing distribution utility demand peaks. The effect of additional PEV battery cycling will affect battery lifetime, and is a function of both the depth of discharge (DOD) and the number of cycles. To analyze the impact of V2G in the urban area distribution utility feeder previously presented, a MATLAB simulation environment was implemented. This environment allows the import of measured demand data, allows the use of different charge and discharge strategies, and the analysis of the influence of the V2G-interactions on the given energy demand profiles. The simulation delivers the possibility to calculate annual costs of battery degradation, energy costs and revenue in relation to parameters like maximum DOD.

Figure 7.13 shows a bar graph of the Eletrosul Headquarters building load curve on a typical weekday, with the three phases shown in blue (Phase 1), red (Phase 2) and green (Phase 3) bars. This public building is representative of office buildings all over the world, where air-conditioning loads occurring in Phase 1 are the single largest load and dictate the curve profile. Solar electricity generation is

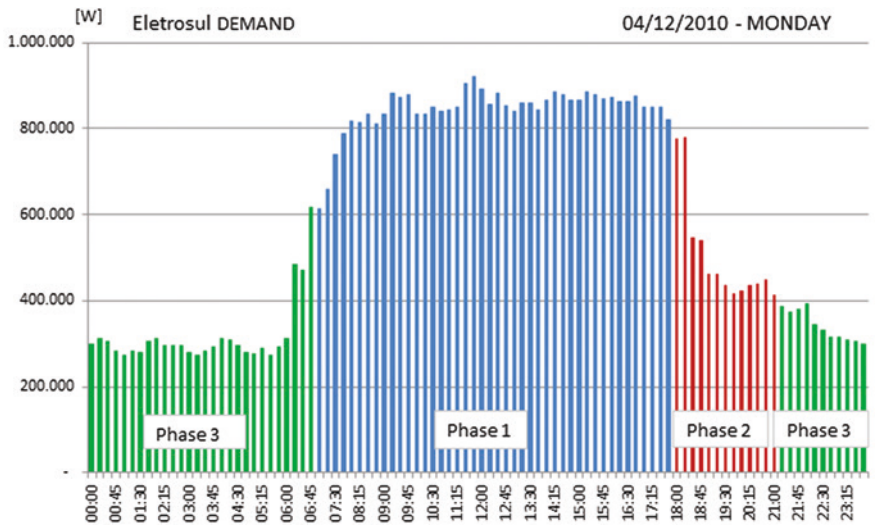

Fig. 7.13 Eletrosul Headquarter building's load curve on a typical weekday, with *Phase 1* dominated by air-conditioning loads during working hours (*blue bars*); *Phase 2*, in the early evening, when distribution utility tariff rates are as high as 10 times the off-peak tariff rates (*red bars*); and *Phase 3*, characterized by low nighttime loads (*green bars*)

reasonably well matched to such a load profile, and PV can effectively assist in shaving the daytime peak. Figure 7.14 shows the PV generation (red bars) for the same day presented in Fig. 7.13 superimposed on the load curve, and Fig. 7.15 shows the bar graph resulting from the PV contribution on the final Eletrosul Headquarter building's load curve.

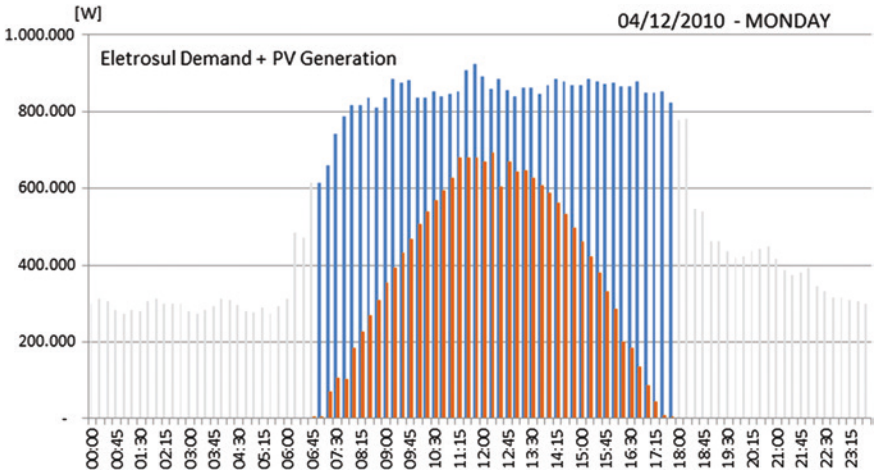

Fig. 7.14 Eletrosul Headquarter building's load curve on a typical weekday, with the one megawatt solar PV generator's contribution (*red bars*) during Phase 1

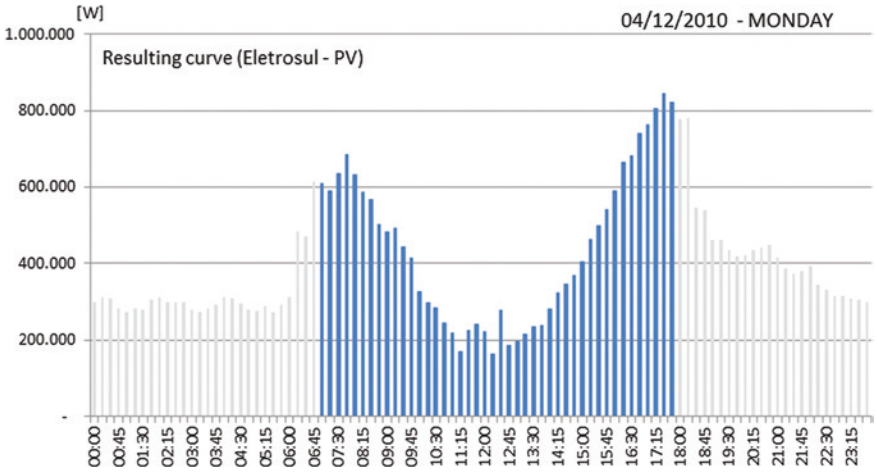

Fig. 7.15 Resulting load curve at the Eletrosul Headquarter building on a typical weekday, with the one megawatt solar PV generator's contribution during Phase 1

Based on the parked and available PEVs that can further assist in modulating this load curve, Fig. 7.16 shows the V2G contribution possible on the same date (red bars), and Fig. 7.17 shows the resulting effect on the Eletrosul Headquarter building's load curve.

In Phase 2, when a number of PEVs owners have arrived home and have plugged their vehicles in onto wall sockets for either recharging the vehicle's

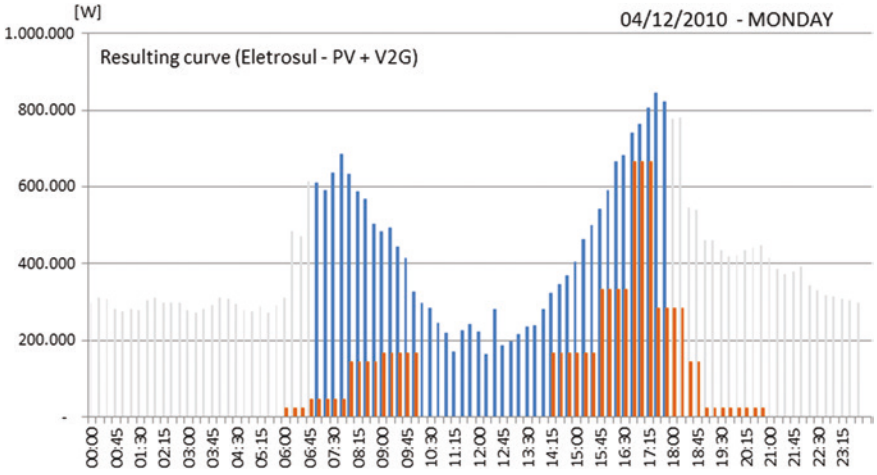

Fig. 7.16 Resulting load curve at the Eletrosul Headquarter building on a typical weekday, with the one megawatt solar PV generator's contribution during Phase 1, and the potential contribution of parked and plugged PEVs available for V2G (*red bars*)

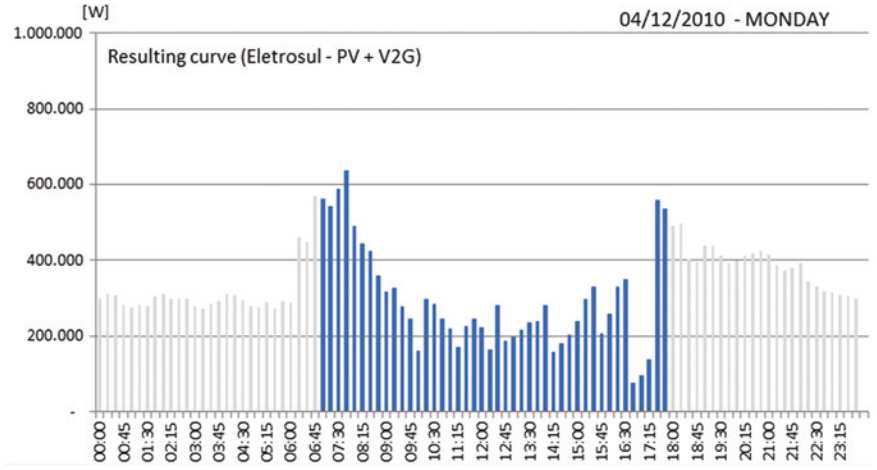

Fig. 7.17 Resulting load curve at the Eletrosul Headquarter building on a typical weekday, with the one megawatt solar PV generator's contribution during Phase 1, and the contribution of parked and plugged PEVs available for V2G

battery or supplying the remaining PEV's energy to the utility grid, a considerable amount of energy can be transferred to the grid via V2G, as the yellow bars in Fig. 7.18 show. In a smart grid environment, PEVs parked at each of these vehicles owners residences can credit the V2G injected power in favor of the Eletrosul Headquarter building. In the late night and early hours, when most of the generation, transmission and distribution assets are idling (Phase 3), the PEV fleet can be recharged with the most inexpensive electricity, as shown in Fig. 7.19.

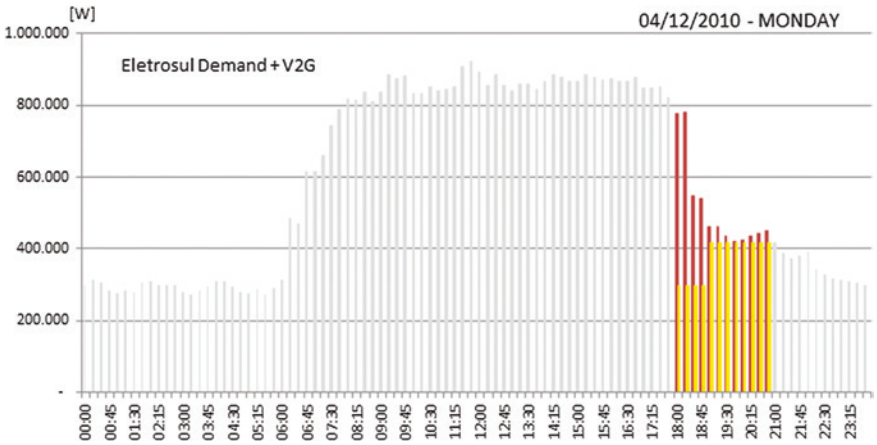

Fig. 7.18 The effect of using V2G electricity from parked and plugged-in PEVs (*yellow bars*) on the Eletrosul Headquarter building's load curve in the early evening (Phase 2) to alleviate power demands from the utility grid

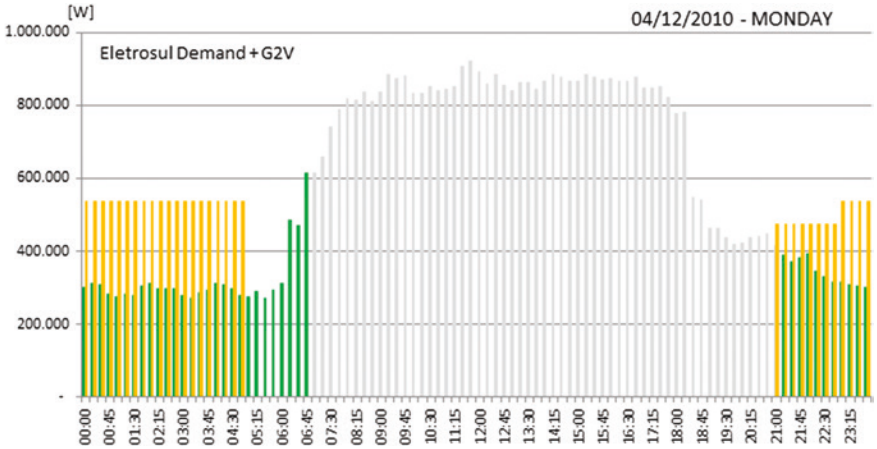

Fig. 7.19 The effect of recharging the parked and plugged-in PEV fleet in the late night and early hours (Phase 3–*yellow bars*) on the Eletrosul Headquarter building's load curve

The combined use of all these strategies can be effectively used to both alleviate the public grid and reduce power demand peaks, as well as provide all the new energy requirements represented by a fleet of PEVs.

The effects of additional charging and discharging PEV batteries in the V2G and G2V context presented previously needs to be further assessed, in order to estimate the costs involved, and a cost-benefits analysis was carried out [40]. It is assumed that PEVs are used during the day for shopping and working, and that they start becoming available for V2G as of 18:00. The shortfall in electrical energy represented by the energy needed to charge the fleet of PEVs driving a given distance per year, is supplied by BIPV and BAPV generators spread on rooftops around the corresponding #TDE05 feeder area, as previously shown. For price calculations the energy price of US$ 0.18/kWh was assumed, including taxes. The assumed car specifications were drawn from [41], as shown in Table 7.1. The battery price assumed from the international market is US$ 300/kWh [42], including taxes. The metering device (US$ 50), a communication device (US$ 50), and the additional hardware needed to allow the feeding of energy to the grid (US$ 33.33/kW) were also assumed including all taxes. All these values are summarized in Table 7.1, and are expected to decrease with technology development and scaling effects. Although the battery efficiency and lifetime both depend on the charge and discharge rate, battery efficiency is assumed at 84 % [43]. It is known that the battery suffers from deep cycling, and that a low DOD will lead to very long battery lifetimes, measured in cycles. This simulation is based on the approach of Rosenkranz and the Fraunhofer ISE's model, as shown in the following equation [41, 44]:

$$N_{\text{Cycles}} = 1331\ \text{DOD}^{-1.8248} \tag{7.8}$$

where N_{Cycles} is the expected battery lifetime in cycles as plotted in Fig. 7.20. This equation leads to an approximately linear dependence of costs per stored energy, depending on the DOD, which can be seen in Fig. 7.21.

The charging and discharging power is limited by the grid connection. In most of the countries, standard plugs allow a maximum current of 10–20 A. Thus we limit the maximum power at $P_{\text{Max}} = 4.4$ kW, based on the standard 20 A sockets, at 220 V. The DC-AC converter efficiency is assumed as $\eta_{\text{converter}} = 98\%$, since state-of-the-art, commercially available inverters for photovoltaic applications reach this efficiency [45]. The efficiencies and power limits are shown in the flow

Table 7.1 Electric vehicle assumed for the simulations in this study (data from Dallinger et al. [41]), shown in both the Brazilian currency R$, and in US$)

Description		Value
Battery capacity		25 kWh
Maximum driving range		200 km
Battery price	R$ 10,201	$ 5,481
Meter for invoicing	R$ 140	$ 75
Communication system	R$ 280	$ 150
Additional electronics	R$ 410	$ 220

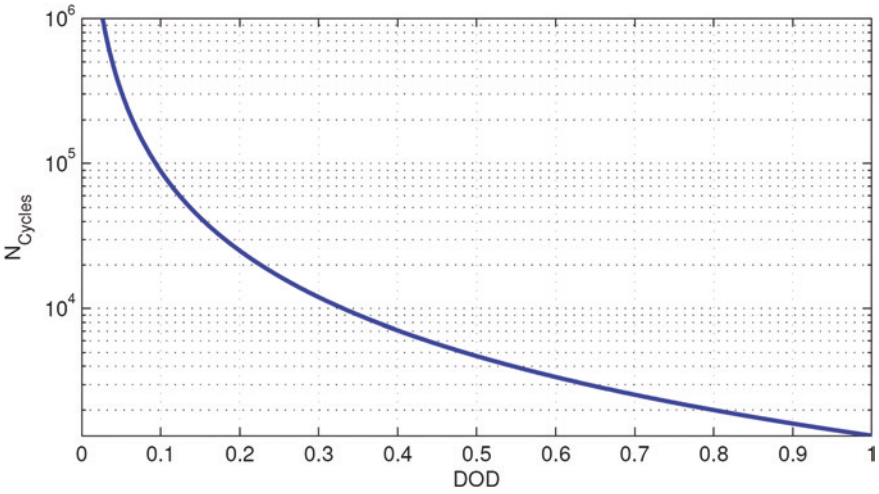

Fig. 7.20 Estimated battery lifetime in cycles, as a function of the depth of discharge-DOD

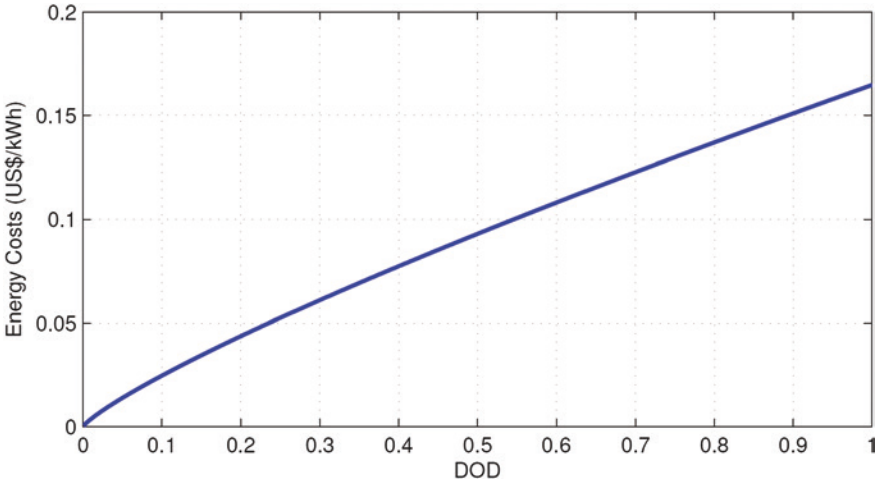

Fig. 7.21 Energy storage costs as a function of the depth of discharge-DOD

diagram in Fig. 7.22. In this figure also the points for P_{Charge} and $P_{Discharge}$ are defined, which will be further defined.

In this simulation, charging is performed between midnight and 6:00 with a charge rate as follows, where E_{SoC} is the energy stored in the battery:

$$P_{Charge}(n) = \min\left(\frac{E_{Capa} - E_{SoC}(n)}{t_{Remaining(n)}}, \eta_{Battery} P_{Max}\right) \tag{7.9}$$

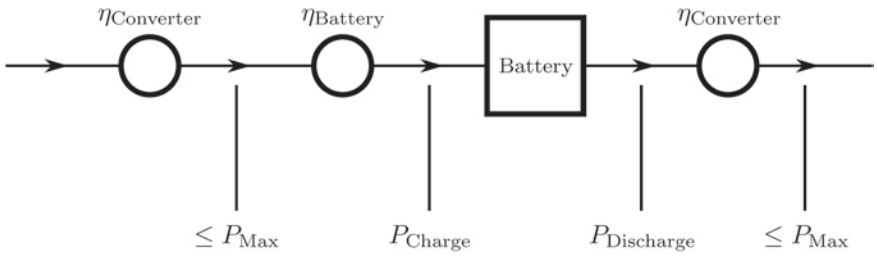

Fig. 7.22 Efficiency and power flows

where $E_{SoC}(n)$ is the energy at the given time-step, in kWh. The value E_{Capa} is the battery capacity drawn from Table 7.1. The value $t_{Remaining(n)}$ is calculated as the time difference between the current time-step and the end of the charge interval, measured in hours.

The new State of Charge (SoC) is therefore

$$E_{SoC}(n+1) = E_{SoC}(n) + P_{Charge}(n)\Delta t \tag{7.10}$$

With time-steps Δt 15 min.

The demand seen by the grid is therefore increased to

$$D_{New}(n) = D_{Old}(n) + \frac{P_{Charge}(n)}{\eta_{Battery}\eta_{Charge}} \tag{7.11}$$

where D_{New} is the resulting demand, and D_{Old} is the original demand, as measured by the distribution utility company.

Everyday, the energy for driving is discharged. With the maximum driving range given in Table 7.1 for the PEV selected for this study, the 200 km result in a driving energy $E_{Drive} = 5$ kWh for average daily driving.

$$E_{SoC}(n+1) = E_{SoC}(n) - E_{Drive} \tag{7.12}$$

While the analysis of daytime charging is outside the scope of the present analysis, in the medium term plugging in might also be possible during the day for staff driving to work every day and parking their cars in assigned parking lots in many public and private, small and large companies. This can also lead to V2G and G2V strategies to assist the public grid when cars remain parked during working hours as previously discussed.

7.3.2.1 Strategy 1: Assumptions for Profit Maximizing with Local Electricity Pricing Model

Distribution utilities around the globe are migrating to a pricing model based on time-of-use for all customers, including residential electricity consumers. To reduce peak demand, a three-level tariff is proposed for residential users. The

energy price during the peak interval from 18:30 to 21:30 is 5x higher than the off-peak price. One hour before and one hour after the peak interval, the energy price is set at 3x higher than during the off-peak period. Together with net-metering regulation for PV generation on individual consumer units, time-of-use tariffs can contribute to grid stabilization when associated with a PEV that is recharged in the early hours (G2V), and assist the utility grid during peak hours in the evenings (V2G). Power trading like proposed by Hartmann and Özdemir [46] can add additional revenue to EV car owners, but in most cases this has been analysed with spot-market prices like the European Energy Exchange (EEX). In Strategy 1, batteries are charged in the morning and energy is sold only during the peak-hours interval, even if the actual demand is already low by any reason. The power being discharged to the grid, shown in Fig. 7.22, is estimated from the available energy and the limits of power electronics:

$$\mathrm{P_{Discharge}\,(n)} = \min\left(\frac{\mathrm{E_{Soc}(n)} - (1 - \mathrm{DOD_{Max}\ E_{Capa}})}{\mathrm{t_{Remaining\ (n)}}},\ \frac{\mathrm{P_{Max}}}{\eta_{\mathrm{Converter}}}\right). \quad (7.13)$$

The parameter $\mathrm{DOD_{MAX}}$ is the maximum allowed DOD, which is going to be varied during different simulations. Here P_{Max} is divided by the converter efficiency $\eta_{\mathrm{Converter}}$, because $\mathrm{P_{Discharge}}$ is measured before the converter, as defined in Fig. 7.22.

The battery charge level is updated according to Eq. 7.14:

$$\mathrm{E_{SoC}(n+1)} = \mathrm{E_{SoC}(n)} - \mathrm{P_{Discharge}(n)} * \Delta\mathrm{t} \quad (7.14)$$

The demand values are, as a consequence, reduced to:

$$\mathrm{D_{New}(n)} = \mathrm{D_{Old}(n)} - \eta_{\mathrm{Battery}} * \mathrm{P_{Discharge}(n)} \quad (7.15)$$

7.3.2.2 Strategy 2: Assumptions for Grid Stabilization

For a fixed number of 250 EVs, as proposed in a recent study carried out in the 2,000 households mixed residential/commercial suburb supplied by feeder #TDE05 [47], a static upper power limit is introduced. These PEVs will dispatch power to the grid to avoid power demands surpassing this upper limit. Applying a merit-order strategy, the upper limit can be interpreted as the point where V2G-energy is cheaper than dispatching other reserves, including transmission and distribution costs, in a strategy designed to avoid overloads and promote grid stabilization. In this case, grid stabilization is a service provided by the car owner to the utility, and the costs for this service are estimated. Discharge power for each car is calculated with a modification of Eq. (7.9). Here Δt is used, because there is no time limitation like in the first strategy:

$$P_{\mathrm{Discharge}}(n) = \min\left(\frac{E_{\mathrm{Soc}}(n) - (1 - \mathrm{DOD_{Max}} E_{\mathrm{Capa}})}{\Delta t},\ \frac{P_{\mathrm{Max}}}{\eta_{\mathrm{Converter}}}\right) \quad (7.16)$$

As many cars as possible discharge with the highest discharge power, which is limited by the grid connection, until the new demand curve is below the upper limit, or there are no more cars available. The battery charge level is updated according to Eq. (7.10). The new demands are calculated as per Eq. (7.11).

Each day the costs for battery degradation by cycling are calculated separately with and without discharge caused by the V2G-service. At first the DOD is calculated

$$D_{New}(n) = 1 - \frac{E_{SoC}(n)}{E_{Capa}} \tag{7.17}$$

Then the number of estimated cycle lifetime N_{Cycles} with the calculated DOD is calculated using Eq. (7.8).

The costs for this discharge are then calculated with

$$Cost_{Degradation}(n) = Cost_{Degradation}(n-1) + \frac{Price_{Battery}}{N_{Cycles}} \tag{7.18}$$

where $Price_{Battery}$ is drawn from Table 7.1. The sums with and without V2G-service are stored separately to be compared afterwards.

In order to supply the new annual energy demands (MWh/year) resulting from a proposed fleet of some 250 EVs in the mixed residential/commercial suburb under study, the incorporation of rooftop PV generators on the single-family houses in the suburb was proposed. We have previously identified the potential of the roofs in that area, which resulted in some 79,000 m^2 of total roof surface, and where more than 50 % of the area are ideally oriented and tilted for receiving at least 95 % of the theoretical maximum solar irradiation daily average density of 4.74 kWh/m^2 [32]. Only areas where at least 1 kWp of PV could be integrated have been used in the simulation, resulting in more than 43,000 m^2, where 7.9 MWp of rooftop PV capacity can be incorporated.

Figure 7.2 has shown the high energy consumption profile during the day (between 8:00 and 18:00), especially during the warmer and sunnier summer months. The seasonality of demand shows a good match with the photovoltaic generation profile; the months with the largest energy demands are also the sunny summer months. Figure 7.23 shows that the integration of PV roofs on residential buildings in the region supplied by feeder #TDE05 can drastically offset the energy consumption especially during summer months. Figure 7.23 also leads to the conclusion that during daytime hours this feeder is able to accommodate these large amounts of photogenerated electricity from grid-connected, rooftop PV generators without the need of any additional distribution system upgrade. The potential of photovoltaic found for the region supplied by the #TDE05 feeder was 7.9 MWp, using high efficiency, commercially available crystalline silicon solar modules, and should be regarded as an upper limit for PV integration in that building stock. The corresponding total annual PV generation expected is just under 8 GWh/year, enough electricity to supply over 4,000 PEV units, each driving more than 12,000 km/year.

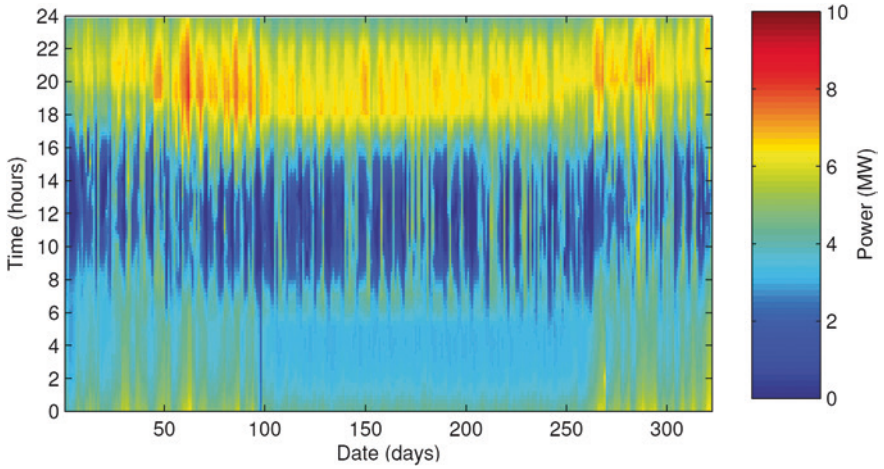

Fig. 7.23 Simulated new demand profile of the #TDE05 feeder with the solar power contribution of 7.9 MWp of PV generators spread over residential rooftops in the corresponding area. Data were calculated using the real demand profile and the corresponding solar irradiation profile for the same period

Braun and Rüther [22] have previously shown the role of grid-connected, building-integrated PV generation in commercial building energy and power loads in a warm and sunny climate. Not only can PV systems installed on residential roofs contribute strategically to alleviate urban distribution networks, shifting peak demand when there is a good correlation between loads and the solar radiation resource availability, but they can also supply all the energy requirements of a number of PEVs that is considerably larger than the number of residential households in the corresponding suburb.

7.3.2.3 Strategy 1: Results for Profit Maximizing with Local Electricity Pricing Model

The strategy of discharging cars only during peak hours in the early evening when tariffs are highest, leads to high revenues for car owners and avoided costs for the distribution utility. This leads to a new demand profile as shown in Fig. 7.24. Unfortunately, and not surprisingly, two new peaks are resulting, right before and right after dispatch, using this V2G grid-support strategy. Figure 7.25 shows the simulated hourly demand profile of the urban feeder #TDE05 resulting from both the 7.9 MWp of PV generation (daytime hours feed-in), and PEVs V2G grid-support in the early evening (during the distribution utility peak hours) for a typical day, as well as the PEVs recharging demands in the early hours (00:00–06:00). It is clear that the PEV contribution in the distribution utility's official early evening peak hours can be anticipated to 18:00 to make an optimized use of the PEVs potential, for a larger number of PEVs might be available for V2G before

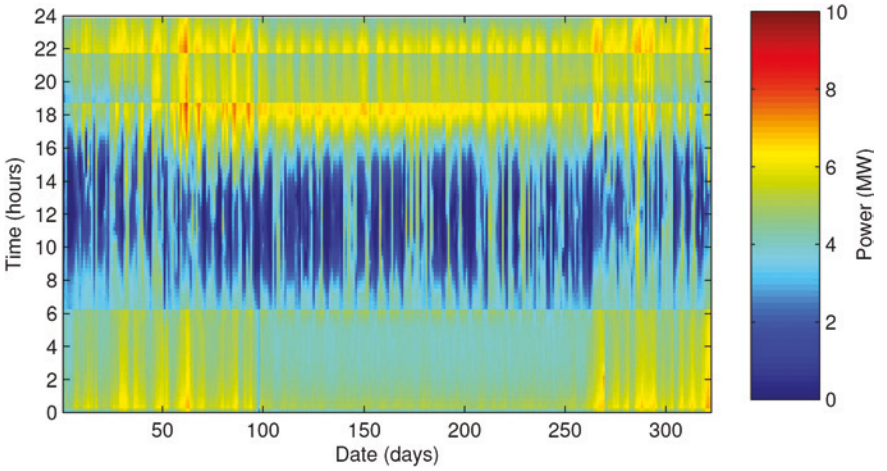

Fig. 7.24 Strategy 1: Simulated demand profile of the #TDE05 feeder, with the new demands represented by the early hours (00:00–06:00) charging of 250 EVs, the contribution of 7.9 MWp of PV generation during daytime hours, and the V2G contribution of the same 250 EV fleet to grid support in the peak hours of the early evening (19:00–21:00) at 75 % maximum DOD

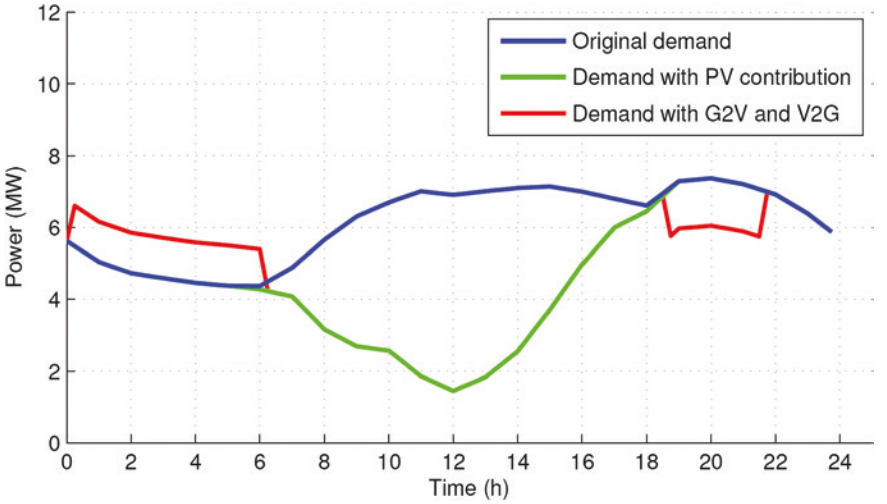

Fig. 7.25 Strategy 1: Simulation example of the new demand profile of the #TDE05 feeder on a typical day, with the new demands represented by the early hours (00:00–06:00) charging of the 250 EVs proposed fleet, the contribution of 7.9 MWp of PV generation during daytime hours, and the V2G contribution of the same 250 EV fleet to grid support in the peak hours of the early evening (19:00–21:00) at 75 % maximum DOD

18:00. The incorporation of PV to generate the new energy demands represented by the new PEV fleet is comfortably accommodated during the daytime hours. Figure 7.24 and 7.25 also show that the early hours recharging of the PEVs has to

be closely monitored to avoid overloading the grid. The new energy demands are represented for a 250 PEVs fleet, which is the optimal value for cars participating in grid stabilization as will be further shown.

The annual revenue as a function of DOD for an individual PEV is plotted in Fig. 7.26. With a DOD of 40 % the revenue already exceeds US$ 1,000 per year, where the annual revenue is calculated as the difference between the annual income and the annual costs. The income does not increase with a higher DOD after 75 %, because of the power limit P_{Max} given by the grid connection, and thus the maximum DOD cannot even be reached.

The costs are the sum of the additional hardware needed for V2G shown in Table 7.1 divided by 10 years, the price of energy recharged for G2V, and the battery degradation caused by V2G, as shown in the stacked area plot in Fig. 7.27. The cost for the grid connection does not increase with increasing the maximum DOD. The money paid for recharged G2V energy rises linearly with increasing the maximum DOD, and reaches a maximum when the power limit of the grid connection is reached. The battery degradation increases nonlinearly with the DOD, as Fig. 7.20 implies.

The time-of-use pricing model shows a large drawback. With an increasing market share of storage using the contract strategy proposed in this work, grid stability will suffer. To point out this effect, the corresponding mean squared error was calculated according to Hartmann and Özdemir [46], as shown in Eq. 7.19, where the upper limit N is the number of time-steps within a year. The mean square is a measure for the deviation between the average demand D_{av} and the current demand D(n). The optimal demand profile is a constant, thus no power margins for higher demands have to be provided. The Mean Square Error (MSE) is zero for $D(n) = D_{av} = \text{const}$.

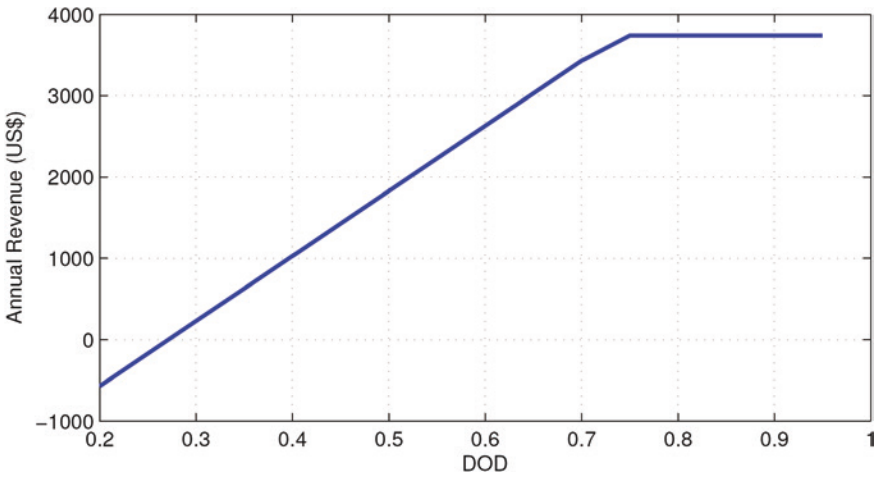

Fig. 7.26 Strategy 1: Annual revenue for one PEV as a function of the DOD with the #TDE05 feeder

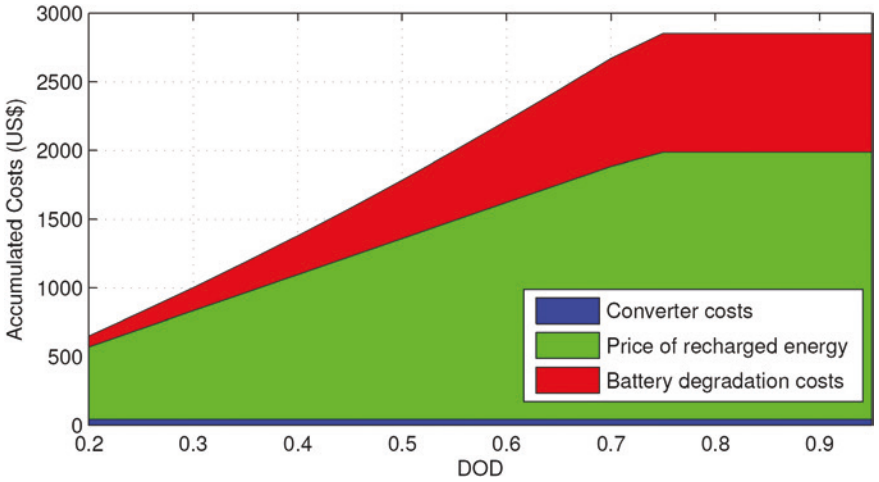

Fig. 7.27 Strategy 1: Accumulated annual costs for V2G and G2V as a function of the DOD for an individual PEV

If the demand varies a lot, a very robust grid with high power reserves has to be established yielding higher investment costs. If there is a high variation in demand, the MSE value is very high as well. Thus a high MSE value is bad for grid stability. The error was calculated for simulations with the number of PEVs varying between 0 and 1,000, and the DOD varying between 0.2 and 1.0. The maximum number of cars analyzed is 1,000, which is a rather high value when compared with the 6,949 residential and 1,099 commercial consumer units in the area.

$$\mathrm{MSE} = \sum_{n=0}^{N} (D(n) - D_{av})^2, \quad N = 30,912 \tag{7.19}$$

The MSE-values are displayed as a color map in Fig. 7.28, where the number of PEVs used is varied along the horizontal axis, and the maximum DOD is varied along the vertical axis. N = 30,912, corresponding to the 15 min time steps over the 8,760–1,032 h (excluding 43 missing days for which no data were available) of the year. The MSE without V2G-activity is calculated as 2.91 MW. Values below this reference point represent a higher grid-stability. It turns out that there is a maximum grid-stability of 2.57 MW, reached with 250 cars and a maximum DOD of 75 %. Thus, optimizing the car owners' revenue does not necessarily increase grid-stability, and these conflicting interests should be properly addressed by government-induced energy policies regarding PEVs and V2G strategies.

In Fig. 7.24 the new demand profile as a result of Strategy 1 was shown. Recharge and discharge intervals are clearly seen as horizontal stripes where the breaks are caused by time-changes because of daylight saving. The figure points out that even during times of low demand, colored in blue, energy is delivered from PEVs to the grid, which does not contribute to grid-stabilization, but generates revenue for the PEV owners.

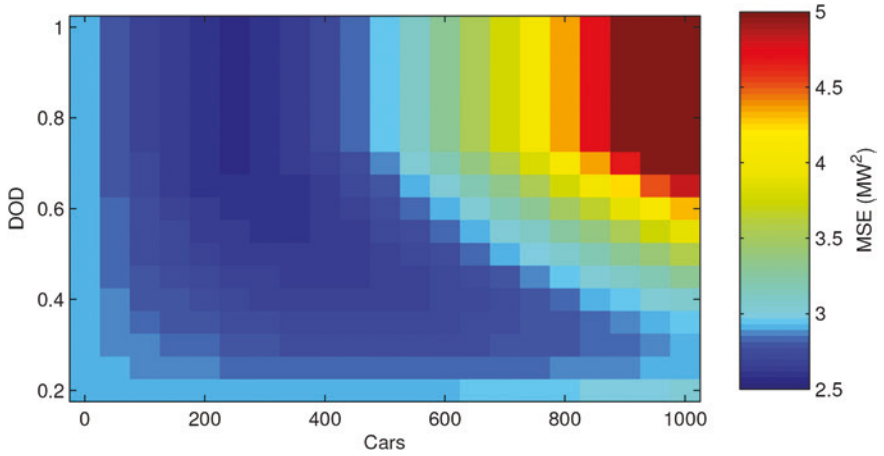

Fig. 7.28 Strategy 1: Mean squared error for different amounts of electric cars and different DOD levels

7.3.2.4 Strategy 2: Results for Grid Stabilization

In Strategy 2 the aim was to stabilize the distribution grid, making more use of the V2G approach by applying a deeper DOD level when necessary, while allowing the #TDE05 feeder to reach the maximum load limit of 6.25 MW before enabling V2G at the utility's peak-hours time. Figure 7.29 shows the resulting effect

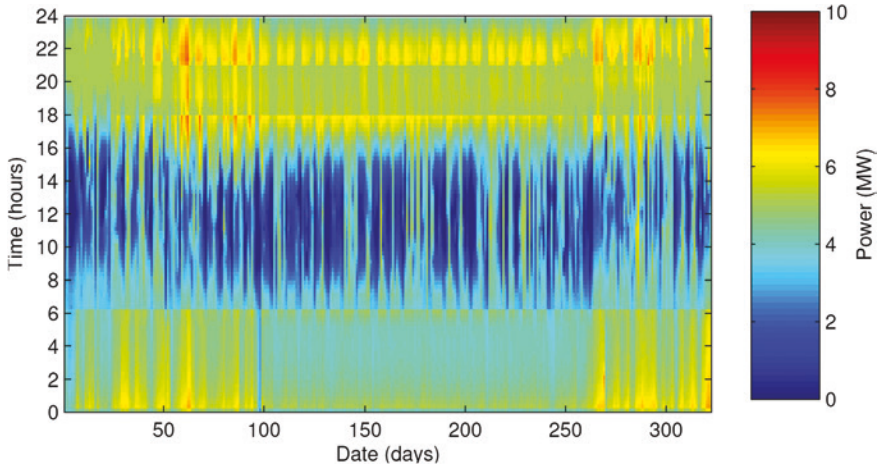

Fig. 7.29 Strategy 2: Simulated demand profile of the #TDE05 feeder with the new demands represented by the early hours (00:00–06:00) charging of 250 PEVs, the contribution of 7.9 MWp of PV generation during daytime hours, and the V2G contribution of the same 250 PEV fleet to grid support in the peak hours of the early evening (19:00–21:00) at 75 % maximum DOD, only when the distribution utility's 6.25 MW upper demand limit is reached

on the feeder's load profile. Figure 7.30 shows the same typical day as Fig. 7.25, using Strategy 2 instead. It shows that there is a lower upper limit and there are no large peaks created by G2V, as seen in Fig. 7.29. Analyzing the demand data with Strategy 2, it turns out that there are several days where the V2G service is not used at all, because the 6.25 MW utility demand limit for feeder #TDE05 is not reached. There is also a small number of days when the PEVs' battery capacity or discharge power limit are not large enough to reduce the demand to the upper limit, resulting in a remaining peak. Nevertheless this strategy will work well, if the dispatch of spinning reserves is more expensive than the dispatch of V2G services. The steep drop in the feeder #TDE05 demand curve at noon shown in Fig. 7.30 indicates a large potential for PEV recharging (G2V) at the workplace for the electric cars fleet.

In this case it also has to be noted that PEV owners' revenue is not maximized, in contrast to Strategy 1. Again the overall grid stability is measured using Eq. (7.19) to compare Strategy 2 with Strategy 1. For 250 electric cars the minimum reachable MSE value is 2.57 MW for Strategy 1, and 2.55 MW for Strategy 2, with an upper limit of 5 MW. Even if this difference is small, better knowledge of driving behavior will lead to greater improvement of MSE values for Strategy 2, but not for Strategy 1. A comparison of different upper limits and their impact on grid stability evaluated with MSE is given in Fig. 7.31, where the upper limit is varied between 4 and 8 MW. It turns out that the PEVs contribute best to grid stabilization in terms of MSE with an upper limit of 5 MW. From the grid operator's

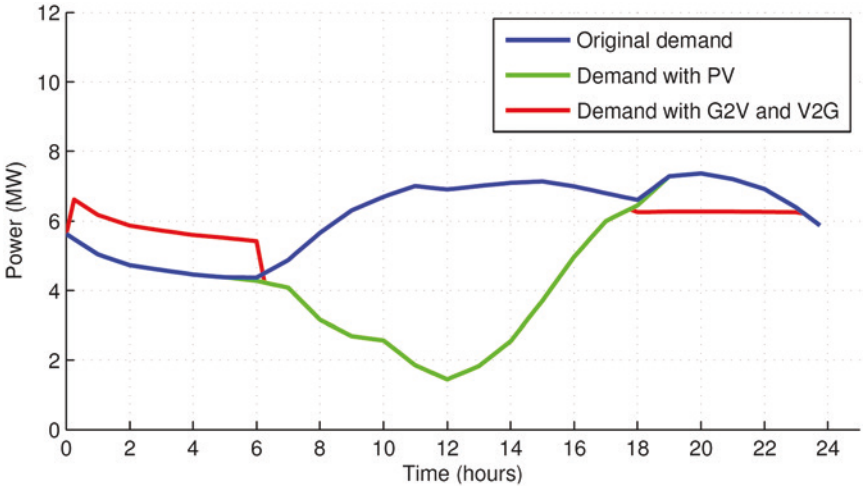

Fig. 7.30 Strategy 2: Simulation example of the new demand profile of the #TDE05 feeder on a typical day, with the new demands represented by the early hours (00:00–06:00) charging of the 250 PEVs proposed fleet, the contribution of 7.9 MWp of PV generation during daytime hours, and the V2G contribution of the same 250 PEV fleet to grid support in the peak hours of the early evening (19:00–21:00) at 75 % maximum DOD, only when the distribution utility's 6.25 MW upper demand limit is reached

perspective, the upper limit should be chosen so that the dispatch of PEVs is cheaper or equal to the dispatch of other resources. Calculating the service costs as the sum over the years of grid connection hardware, costs for efficiency losses and battery degradation divided by V2G energy delivered, leads to Fig. 7.32. It can be observed that the service cost per delivered energy is very high for a high upper limit, because the fixed costs have to be covered without selling large amounts of energy to the grid. Furthermore the service cost for low upper limits is high,

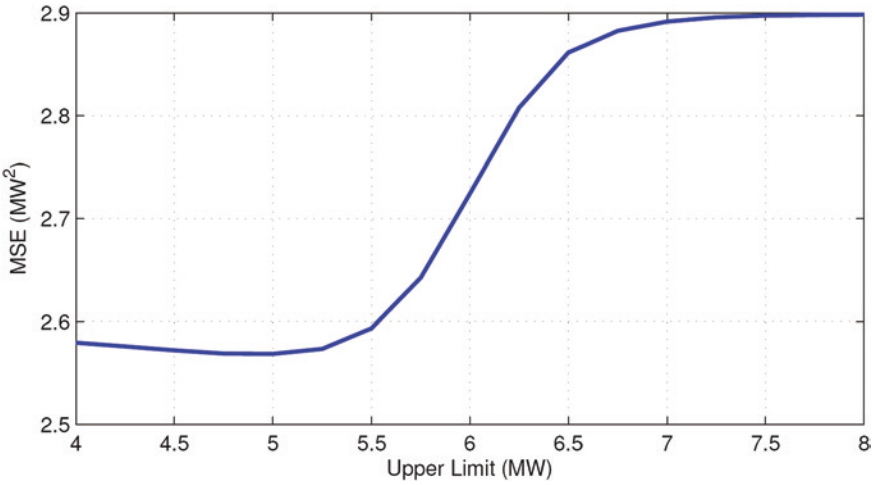

Fig. 7.31 Strategy 2: Grid stability as a function of the upper limit (in MW), where V2G is active with 250 PEVs participating in grid stabilization, and a 75 % maximum DOD level

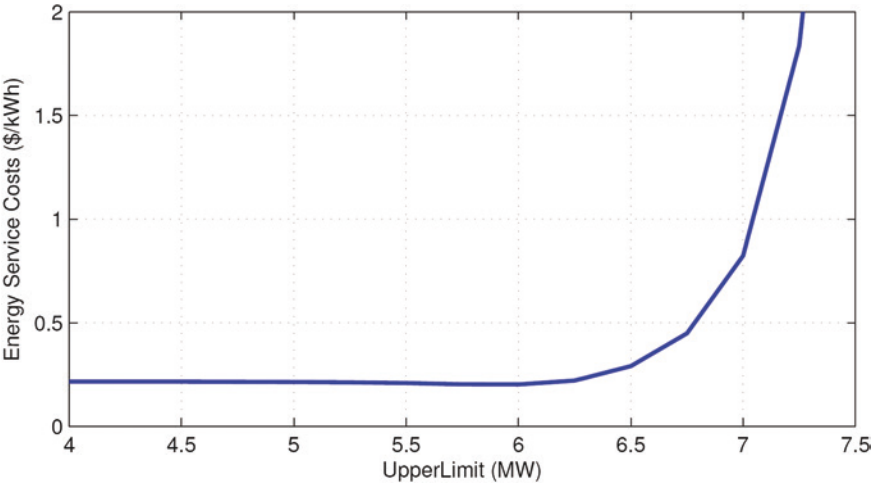

Fig. 7.32 Strategy 2: Service costs for V2G service for each PEV per energy as a function of the upper limit where V2G is active, and a 75 % maximum DOD level

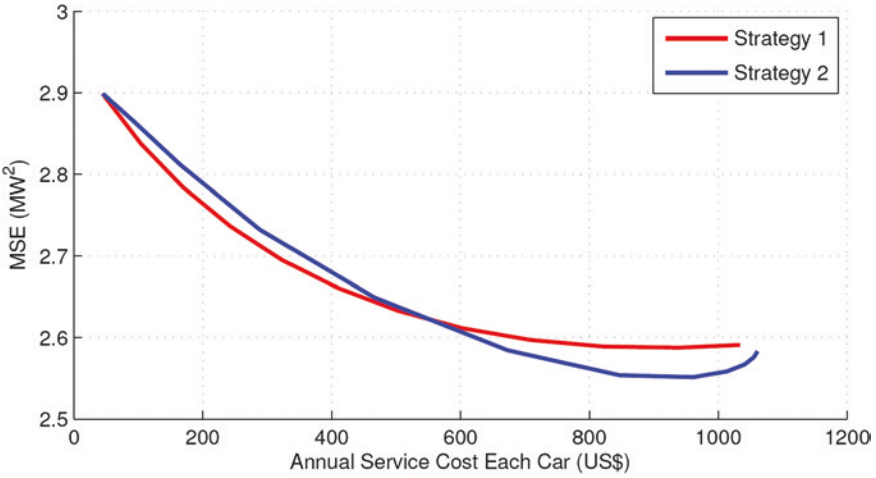

Fig. 7.33 Comparison between Strategy 1 and Strategy 2 regarding MSE, plotted as a function of annual costs per PEV including all V2G hardware, battery degradation and energy losses

because of intensive battery degradation. Comparing Figs. 7.31 and 7.32, it turns out that a reasonable compromise between costs and grid stability can be observed between 4.0 and 5.5 MW.

To compare both strategies, the MSE was plotted in Fig. 7.33 as a function of the annual service cost per PEV. It can be observed that using Strategy 2, a lower MSE, and thus a higher grid stability, can be achieved. In addition, Strategy 2 fits well in the concept of merit order, whereas Strategy 1 does not. In Fig. 7.29 new energy demands caused by Strategy 2 are exposed. During times of low demands, no energy is delivered to the grid. During times of high demands, peaks are shaved to the upper limit of 5–6 MW. In times of extraordinary high demands, battery capacity even at high DOD levels is not enough to shave peaks sufficiently, as seen during the days 61 and 62 at night in Fig. 7.29.

7.3.2.5 Energy Balance

In this section an overall energy balance is discussed. Both Tables 7.2 and 7.3 present the energy balance along the year for Strategy 1 and Strategy 2 respectively. Table 7.2 shows the energy balance considering Strategy 1, with 250 electric cars participating in grid stabilization, with a 75 % maximum DOD level, as well as the PV contribution of 7.9 MWp of rooftop generators spread all over the metropolitan region supplied by the #TDE05 feeder. Photovoltaic energy is sufficient to compensate for energy losses due to conversion and battery cycling efficiency, as well as the energy demands caused by PEV driving. As expected, PV energy generation is higher in the summer season, and thus the balanced energy is high during December and January. Over the year, Strategy 1 leads to 1,063 MWh of

Table 7.2 Energy balance for strategy 1

Months	Valid days	V2G (MWh)	G2V (MWh)	PV (MWh)	Balance (MWh)
January	29	95.7	158.6	799.7	736.9
February	28	92.4	157.1	689.0	624.4
March	29	95.7	162.7	838.5	771.6
April	29	95.7	162.7	748.6	681.6
May	31	102.3	173.9	682.8	611.1
June	18	59.4	101.0	411.3	369.8
July	16	52.8	89.7	293.8	256.8
August	24	79.2	134.6	609.7	554.3
September	27	89.1	151.4	491.3	429.0
October	30	99.0	168.3	664.6	595.3
November	30	99.0	168.3	797.1	727.9
December	31	102.3	173.9	837.2	765.6
Annual		1,062.6	1,802.2	7,863.6	7,124.0

Balance: (V2G + PV − G2V) Rows and columns may not add horizontally or vertically due to rounding

Table 7.3 Energy balance for strategy 2

Months	Valid days	V2G (MWh)	G2V (MWh)	PV (MWh)	Balance (MWh)
January	29	64.3	119.6	799.7	744.4
February	28	88.0	151.7	689.0	625.3
March	29	97.7	165.1	838.5	771.1
April	29	91.4	157.3	748.6	682.7
May	31	102.3	173.8	682.8	611.3
June	18	59.0	100.4	411.3	369.9
July	16	53.9	91.1	293.8	256.6
August	24	80.8	136.7	609.7	553.8
September	27	89.0	151.3	491.3	429.0
October	30	20.4	165.6	664.6	519.4
November	30	96.9	168.7	797.1	725.3
December	31	93.0	166.0	837.2	764.2
Annual		936.7	1,747.3	7,863.6	7,053.0

Balance: (V2G + PV − G2V) Rows and columns may not add horizontally or vertically due to rounding

electricity supplied to the grid with V2G, 1,801 MWh of electricity drawn from the grid with G2V, and 7,863 MWh of electricity generated by the 7.9 MWp of PV rooftops. There is therefore a considerably large positive annual balance of electricity fed to the public grid (V2G + PV generation − G2V) of 7,124 MWh.

In Table 7.3 the energy balance for Strategy 2 with 250 cars participating in grid stabilization, a 75 % maximum DOD level, the PV contribution of 7.9 MWp of

rooftop generators spread all over the metropolitan region supplied by the #TDE05 feeder, and an upper limit of 5 MW for the feeder demand is presented. It turns out that the overall energy gain is larger than with Strategy 1. Strategy 1 is optimized for electric car owners' revenues, and the losses are thus not necessarily minimized. With Strategy 2 fewer losses occur because the V2G option is used only to stabilize the grid, and not to maximize car owners' revenues. Over the year, Strategy 2 leads to 936 MWh of electricity supplied to the grid with V2G, 1,747 MWh of electricity drawn from the grid with G2V, and the same 7,863 MWh of electricity generated by the 7.9 MWp of PV rooftops. The positive annual balance of electricity fed to the public grid (V2G + PV generation − G2V) is in this case very similar to the one resulting from Strategy 1, totaling 7,053 MWh. In both cases, the surplus electricity generated by making use of the full PV potential of the local residential rooftops is enough to feed a PEV fleet of some 4,000 cars.

7.4 Conclusions

In this chapter the potential of using PEVs and onsite solar PV generation in a smart grid environment, to both assist peak demand reduction in urban utility grids and to supply the additional energy requirements of a PEV fleet were assessed. Real electricity demand data, and real local solar irradiation and PV generation data were used to assess the potential contribution of using both V2G and PV generation strategies to assist the distribution utility #TDE05 feeder in peak shaving in the early evening. Commercial/public building and detached, single-family residential building rooftop PV generation spread over the area supplied by this utility feeder allowed to produce electricity well in excess of the additional amounts of electricity required by a number of PEVs to be owned by a fraction of the local residents. On the basis of a simulation with time-steps of one hour using measured demand data, PV systems have shown to have the potential to reduce load fluctuations in the urban grid. The power generated correlates well with the demand data and might thus reduce the daytime demand peak. A 7.9 MWp PV system installed in the urban region shown here can compensate the consumption of air-conditioning in the commercial buildings. This analysis points out that there is a potential for PEVs to stabilize the grid in regards of peak load shaving. The introduction of time-of-use distribution utility tariffs, with higher energy prices at peak times also for residential consumers, should in fact result in reduced demand during peak time, but might also create new peaks around this time interval. As shown with Strategy 1, assumed there is a net metering contract, this policy might be exploited leading to revenues for PEV owners, but not necessarily to grid stabilization. This effect is sensitive to the number of PEVs into consideration. The second strategy, with a fixed limit, allows for the concept of merit order, and is therefore more suitable for the utility. To make use of this strategy, PEV owners would need to receive a small reward just for having the car connected to the grid. Only in rare cases, when demand exceeds a specific limit, the stored energy would be solicited by the utility.

References

1. Kempton W, Letendre SE (1997) Electric vehicles as a new power source for electric utilities. Transp Res Part D Transp Environ 2:157–175
2. Kempton W, Kubo T (2000) Electric-drive vehicles for peak power in Japan. Energy Policy 28:9–18
3. Kempton W, Tomić J (2005) Vehicle-to-grid power fundamentals: calculating capacity and net revenue. J Power Sources 144:268–279
4. Kempton W, Tomić J (2005) Vehicle-to-grid power implementation: from stabilising the grid to supporting large-scale renewable energy. J Power Sources 144:280–294
5. REN21. Renewables (2014) Global Status Report (Paris: REN21 Secretariat) 2014. Available at www.ren21.net
6. Mints P. PV Costs/ASPs/Shipments & Cost Price Delta, 2003–2014. Solar Flare, Issue 1, 2014
7. Rüther R, Zilles R (2011) Making the case for grid-connected photovoltaics in Brazil. Energy Policy 39:1027–1030
8. Perez R, Seals R, Herig C (1996) PV can add capacity for the grid. NREL Publications, Golden, USA. DOC/GO-10096-262
9. Perez R, Letendre S, Herig C (2001) PV and grid reliability: availability of PV power during capacity shortfalls. In: Proceedings of the American Solar Energy Society—ASES annual conference, Washington, DC, pp 1–4
10. Jardim CS, Rüther R, Salamoni IT, Viana TS, Rebechi SH, Knob PJ (2008) The strategic siting and the roofing area requirements of building-integrated photovoltaic solar energy generators in urban areas in Brazil. Energy Build 40:365–370
11. Méndez VH, Rivier J, de la Fuente JI, Gómez T, Arceluz J, Marín J, Madurga A (2006) Impact of distributed generation on distribution investment deferral. Electr Power Energy Syst 28:244–252
12. Jimenez H, Calleja H, González R, Huacuz J, Lagunas J (2006) The impact of photovoltaic systems on distribution transformer: a case study. Energy Convers Manag 47:311–321
13. Rüther R, Knob PJ, Jardim CS, Rebechi SH (2008) Potential of building-integrated photovoltaic solar energy generators in assisting daytime feeders in urban areas in Brazil. Energy Convers Manag 49:1074–1079
14. Naspolini HF, Militão HSG, Rüther R (2010) The role and benefits of solar water heating in the energy demands of low-income dwellings in Brazil. Energy Convers Manag 51:2835–2845
15. Naspolini HF, Rüther R (2011) The impacts of solar water heating in low-income households on the distribution utility's active, reactive and apparent power demands. Sol Energy 85:2023–2032
16. Rüther R, Pereira Junior LC, Pfitscher PH, Viana TS (2011) Assessing the potential of electric vehicles and photovoltaics in a smart-grid environment in Brazil. In: Proceedings of the 3rd European conference on smart-grids and e-mobility, pp 172–179
17. Zahedi A (2006) Solar photovoltaic (PV) energy; latest developments in the building integrated and hybrid PV systems. Renew Energy 31:711–718
18. Urbanetz J, Zomer CD, Rüther R (2011) Compromises between form and function in grid-connected, building-integrated photovoltaics (BIPV) at low-latitude sites. Build Environ 46:2107–2113
19. Ordenes M, Marinoski DL, Braun P, Rüther R (2007) The impact of building-integrated photovoltaics on the energy demand of multi-family dwellings in Brazil. Energy Build 39:629–642
20. Rüther R, Braun P (2009) Energetic contribution potential of building-integrated photovoltaics on airports in warm climates. Sol Energy 83:1923–1931
21. Heipled S, Sailor DJ (2008) Using building energy simulation and geospatial modeling techniques to determine high resolution building sector energy consumption profiles. Energy Build 40:1426–1436

22. Braun P, Rüther R (2010) The role of grid-connected, building-integrated photovoltaic generation in commercial building energy and power loads in a warm and sunny climate. Energy Convers Manag 51:2457–2466
23. Chan AT, Yeung VCH (2005) Implementing building energy codes in Hong Kong: energy savings, environmental impacts and cost. Energy Build 37:631–642
24. Brogren M, Green A (2003) Hammarby Sjostad—an interdisciplinary case study of the integration of photovoltaics in a new ecologically sustainable residential area in Stockholm. Sol Energy Mater Sol Cells 75:761–765
25. Burger B, Rüther R (2006) Inverter sizing of grid-connected photovoltaic systems in the light of local solar resource distribution characteristics and temperature. Sol Energy 80:32–45
26. Jones DL, Hattersley L, Ager R (2000) Photovoltaics in buildings BIPV projects. Energy Technology Support Unit (ETSU), Harwell (United Kingdom) Department of trade and industry. Available at www.opengrey.eu/partner/bldsc
27. Pantic S, Candanedo L, Athienitis AK (2010) Modeling of energy performance of a house with three configurations of building-integrated photovoltaic/thermal systems. Energy Build 42:1779–1789
28. Parker DS (2009) Very low energy homes in the United States: perspectives on performance from measured data. Energy Build 41:512–520
29. Penga C, Huanga Y, Wub Z (2011) Building-integrated photovoltaics (BIPV) in architectural design in China. Energy Build 43:3592–3598
30. Sun LL, Yang HX (2010) Impacts of the shading-type building-integrated photovoltaic claddings on electricity generation and cooling load component through shaded windows. Energy Build 42:455–460
31. Mardaljevic J, Rylatt M (2003) Irradiation mapping of complex urban environments: an image-based approach. Energy Build 35:27–35
32. Santos IP, Rüther R (2012) The potential od building-integrated (BIPV) and building-applied photovoltaics (BAPV) in single-family, urban residences at low latitudes in Brazil. Energy Build 50:290–297
33. Rüther R (1998) Experiences and operational results of the first grid-connected, building-integrated thin film photovoltaic installation in Brazil. In: Proceedings of the 2nd world conference and exhibition of photovoltaic solar energy convertion, Vienna, Austria, pp 2655–2658
34. Rüther R, Dacoregio MM (2000) Performance assessment of a 2kWp grid-connected, building-integrated, amorphous silicon photovoltaic installation in Brazil. Prog Photovolt Res Appl 7:257–266
35. Stabler DL, Wronski CR (1977) Reversible conductive charges in this charge produced amorphous silicon. Appl Phys Lett 31:292–294
36. Rüther R, Livingstone J (1994) Seasonal variations in amorphous silicon solar module outputs and thin film characteristics. Sol Energy Mater Sol Cells 36:29–43
37. Rüther R (1999) Demonstrating the superior performance of thin-film, amorphous silicon for building-integrated PV systems in warm climates. In: Proceedings of the international solar energy society's solar world congress. ISES, Jerusalem, Israel, pp 221–224
38. Radiasol, Laboratório de Energia Solar—GESTE—PROMEC, Porto Alegre. Available at www.solar.ufrgs.br
39. SWERA (2011) Solar and wind energy resource assessment programme, UNEP 2011. Available at http://swera.unep.net/
40. Drude L, Pereira Junior LC, Rüther R (2014) Photovoltaics and electric vehicle-to-grid (V2G) strategies for peak demand reduction in urban regions in Brazil in a smart grid environment. Renew Energy 68:443–451
41. Dallinger D, Krampe D, Wietschel M (2010) Vehicle-to-grid regulation based on a dynamic simulation of mobility behavior. Fraunhofer Institute for Systems and Innovation Research (ISI), Working Papers Sustainability and Innovation S4/2010
42. Tomić J, Kempton W (2007) Using fleets of electric-drive vehicles for grid support. J Power Sources 168:459–468

43. Biere D, Dallinger D, Wietschel M (2009) Ökonomische analyse der erstnutzer von elektrofahrzeugen. Zeitschrift für Energiewirtschaft 33:173–181
44. Rosenkranz C (2003) Deep cycle batteries for plug-in hybrid application. EVS-20 Plug-in Hybrid Workshop, Long Island-CA, United States
45. Meinhardt M (2007) Pv-systemtechnik—ein motor der kostenreduktion für die photovoltaische stromerzeugung. SMA Technologie AG, Niestetal. Available at www.fvsonnenenergie.de/fileadmin/publikationen/tmp_vortraege_jt2007/th2007_15_meinhardt.pdf2241
46. Hartmann N, Özdemir E (2011) Impact of different utilization scenarios of electric vehicles on the german grid in 2030. J Power Sources 196:2311–2318
47. Pereira Junior LC (2011) A interação entre geradores solares fotovoltaicos e veículos elétricos conectados à rede elétrica pública. Master's thesis, Universidade Federal de Santa Catarina, Florianópolis-SC